© 2022. Published by The Company of Biologists Ltd | Journal of Cell Science (2022) 135, jcs259493. doi:10.1242/jcs.259493

RESEARCH ARTICLE

Emerin regulation of nuclear stiffness is required for fast amoeboid migration in confined environments

Sandrine B. Lavenus*, Karl W. Vosatka, Alexa P. Caruso, Maria F. Ullo‡, Ayesha Khan and Jeremy S. Logue§

ABSTRACT

When metastasizing, tumor cells must traverse environments with diverse physicochemical properties. Recently, the cell nucleus has emerged as a major regulator of the transition from mesenchymal to fast amoeboid (leader bleb-based) migration. Here, we demonstrate that increasing nuclear stiffness through elevating lamin A, inhibits fast amoeboid migration in melanoma cells. Importantly, nuclei may respond to force through stiffening. A key factor in this process is the inner nuclear membrane (INM) protein emerin. Accordingly, we determined the role of emerin in regulating fast amoeboid migration. Strikingly, we found that both the up- and downregulation of emerin results in an inhibition of fast amoeboid migration. However, when key Src phosphorylation sites were removed, upregulation of emerin no longer inhibited fast amoeboid migration. Interestingly, as measured by using a Src biosensor, activity of Src was low in cells within a confined environment. Thus, the fast amoeboid migration of melanoma cells depends on the precise calibration of emerin activity.

KEY WORDS: Cancer, Metastasis, Cell migration, Cytoskeleton, Nucleus, Nuclear envelope, Emerin, Src, Mechanotransduction

INTRODUCTION

Cell migration is integral to embryonic development, immune surveillance and wound healing. When de-regulated, cell migration may also contribute to disease. In transformed cells, cell migration is an essential aspect of metastasis, which accounts for the vast majority of cancer deaths. Accordingly, elucidating the molecular mechanisms that regulate the migration of cancer cells may lead to the development of life-saving therapeutics.

It has become clear that cancer cells may utilize several mechanisms to disseminate from a primary tumor to distant tissues. This includes mesenchymal, collective, lobopodial, osmotic engine and fast amoeboid (leader bleb-based) migration (Paul et al., 2017; Yamada and Sixt, 2019). Osmotic engine and leader bleb-based migration (LBBM) occurs specifically within confined environments, such as along or within micro-capillaries/lymphatics and between epithelial surfaces (Logue et al., 2015; Stroka et al., 2014). During LBBM, cells protrude a large and intracellular pressure-driven plasma membrane (PM) bleb (Liu et al., 2015; Logue et al., 2015; Ruprecht et al., 2015). Because cells migrate in the direction of this bleb, it was termed a 'leader bleb' (Logue et al., 2015). With non-specific friction, a rapid cortical actin flow in leader blebs provides the motive force for cell movement (Bergert et al., 2015). Because it only requires non-specific friction, cells may use LBBM in diverse physiochemical environments (Madsen and Sahai, 2010). This property is likely to promote distant metastasis. A phenotypically similar mode of migration has been observed in breast and melanoma tumors by intravital imaging (Tozluoğlu et al., 2013). Notably, amoeboid migrating melanoma cells have also been observed at the invasive fronts of patient tumors (Cantelli et al., 2015).

Because cancer cells may adopt multiple mechanisms of migration, preventing or abating metastasis by using therapeutics is challenging. For instance, we have previously demonstrated that fast amoeboid migrating cells are resistant to Src inhibitors (Logue et al., 2018; Ullo and Logue, 2018). This is in contrast to mesenchymal migration, which requires Src activity to form focal adhesions (Webb et al., 2004). Therefore, the identification of factors required by all modes of cancer cell migration is necessary for the development of effective therapeutics. Within tissues, motile cells must deform in order to squeeze through confining environments. Therefore, factors that regulate cell deformability might be ideal therapeutic targets.

In recent years, it has become clear that the nucleus plays an integral role in sensing the cellular environment. In a confined cell, it has been demonstrated that the nuclear membrane becomes tensed, which together with increased intracellular Ca^{2+}, recruits cytosolic phospholipase A2 (cPLA2, also known as PLA2G4A) (Lomakin et al., 2020; Venturini et al., 2020). At the nuclear membrane, cPLA2 liberates arachidonic acid to increase actomyosin contractility (Gong et al., 1992). Intracellular Ca^{2+} is released upon rupture of the ER, which becomes compressed between the nucleus and PM in confined cells (Lomakin et al., 2020; Venturini et al., 2020). Thus, cPLA2 regulates the phenotypic transition from mesenchymal to fast amoeboid migration in confined environments.

Because of the essential role of nuclear membrane tension, factors that regulate the deformability of the nucleus are likely to be potent regulators of fast amoeboid migration. Accordingly, we set out to determine the role of the inner nuclear membrane (INM) protein emerin in regulating fast amoeboid migration. Emerin is a LAP2, emerin, MAN1 (LEM) domain-containing protein, which connects emerin to chromatin through direct interaction with barrier-to-autointegration factor (BAF, also known as BANF1) (Berk et al., 2013). Interestingly, it has been demonstrated that emerin confers nuclear adaptation to force. More specifically, when using magnetic beads coated with anti-nesprin-1 antibody and isolated nuclei, repeated pulling using magnetic tweezers led to nuclear stiffening in an emerin-dependent manner (Guilluy et al., 2014). Additionally, this effect was found to depend on phosphorylation of emerin at residues Y74 and Y95 by Src (Guilluy et al., 2014). Thus, emerin may protect nuclei from rupture when subjected to repeated pulling forces.

Department of Regenerative and Cancer Cell Biology, Albany Medical College, 47 New Scotland Ave, Albany, NY 12208, USA.
*Present address: Regeneron Pharmaceuticals, 81 Columbia Turnpike, Rensselaer, NY 12144, USA. ‡Present address: Massachusetts Institute of Technology, Department of Biology, 31 Ames St, Cambridge, MA 02142, USA.

§Author for correspondence (loguej@amc.edu)

J.S.L., 0000-0002-5274-2052

Handling Editor: Michael Way
Received 20 October 2021; Accepted 17 March 2022

Journal of Cell Science (2022) 135, jcs259493. doi:10.1242/jcs.259493

Here, we report that emerin activity was precisely calibrated in melanoma cells for fast amoeboid (leader bleb-based) migration. Using isolated nuclei, we found that nuclei were softest at intermediate levels of emerin. Surprisingly, Src activity was found to be reduced in confined cells, as measured by using a fluorescence resonance energy transfer (FRET) biosensor. Thus, nuclear deformability in melanoma cells may be enhanced by the downregulation of Src.

RESULTS

Using human malignant melanoma A375-M2 cells, we set out to determine how components of the nuclear lamina regulate fast amoeboid migration (Clark et al., 2000). To simulate the mechanical (compressive) forces in tissues, we subjected cells to an assay that has been decribed in detail elsewhere (https://protocolexchange.researchsquare.com/article/nprot-6585/v1). Briefly, cells are placed under a slab of polydimethylsiloxane (PDMS), which is held at a defined height above cover glass by micron-sized beads. Both the PDMS and cover glass is coated with bovine serum albumin (BSA; 1%), which provides friction for cell movement (Bergert et al., 2015). Using a range of cell types, it has been shown that confining cells down to a maximum height of 3 µm is most effective in converting cells to fast amoeboid migration (Liu et al., 2015). Notably, the phenotypes observed *in vitro* are highly similar to what has been observed *in vivo* (Tozluoğlu et al., 2013). Using this assay, we observed three distinct phenotypes, which we termed leader mobile (LM), leader non-mobile (LNM) and no leader (NL) (Fig. 1A and Movies 1-3). The LNM fraction represents cells that form leader blebs, which are stable over time, but do not move. NL cells are also non-mobile. Interestingly, for all phenotypes the nucleus underwent rapid shape changes (Fig. 1A; green channel). As a key component of the lamin nuclear skeleton, lamin A levels have been shown to correlate with nuclear stiffness (Lammerding et al., 2006). Therefore, we wondered whether increased levels of lamin A would prevent nuclear membrane stretch and the activation of mechanosensing enzymes, such as cPLA2 (Lomakin et al., 2020; Venturini et al., 2020). In agreement with this concept, cells with increased lamin A had nuclei that were rounder and less frequently in leader blebs (Fig. 1B,C). The presence of the nucleus in leader blebs correlates with increased migration speed (https://protocolexchange.researchsquare.com/article/nprot-6585/v1; Liu et al., 2015). Compared to cells expressing enhanced green fluorescent protein (EGFP) alone, cells overexpressing mEmerald-tagged lamin A [lamin A-mEmerald; lamin A overexpression (OE)] were significantly slower (Fig. 1D). Moreover, when separated by phenotype, lamin A OE cells were less likely to be mobile (Fig. 1E). However, the speed of mobile cells was unaffected by lamin A OE (Fig. 1F). Therefore, the transition to the leader mobile (LM) phenotype was inhibited by lamin A OE. Interestingly, lamin A OE led to a ∼50% reduction in leader bleb area (Fig. 1G). Lamin A was found to be ∼1.5 fold overexpressed in transfected cells, as measured by immunofluorescence (IF; Fig. 1H). In contrast, RNA interference (RNAi) of lamin A increased the leader bleb area (Fig. S1A-H). These results are consistent with a model in which the nuclear membrane stretch regulates actomyosin contractility through cPLA2. Thus, increasing levels of lamin A correlate with increased nuclear stiffness and a reduction in motility (Fig. 1I). Using transmigration assays, we confirmed that the nuclear membrane tension sensor cPLA2 is required for confined migration in melanoma cells. More specifically, upon RNAi of cPLA2, transmigration through 8 µm pores was reduced by ∼50%, whereas transmigration through 12 µm pores was unaffected (Fig. 1J).

The inner nuclear membrane (INM) protein emerin has been found to stiffen the nucleus in response to force (Guilluy et al., 2014). It has been proposed that emerin regulates nuclear stiffness through interactions with lamin A (Berk et al., 2013). Initially, we wondered how cells would respond to the up- and downregulation of emerin. Using emerin tagged with EGFP (emerin-EGFP; emerin OE), we found emerin to be enriched at the nuclear envelope and ER of melanoma cells (Fig. 2A; green channel). In response to either upregulation (emerin OE) or downregulation of emerin (RNAi), nuclei were rounder and less often present in leader blebs (Fig. 2B,C and Fig. S1A). Similarly, each condition led to significant decreases in cell speed and a reduction on the proportion of mobile cells (Fig. 2D-F). While RNAi of emerin led to a modest decrease in leader bleb area, emerin OE reduced leader bleb area by ∼50% (Fig. 2G and Movie 4). Emerin was found to be ∼2 fold overexpressed in transfected cells, as measured by IF (Fig. 2H). Collectively, these data suggest that fast amoeboid migration requires an intermediate level of emerin (Fig. 2I). Emerin RNAi led to a significant decrease in transmigration through 8 µm pores, whereas transmigration through 12 µm pores was unaffected (Fig. 2J). In emerin and cPLA2 RNAi cells, transmigration rates were reduced to a similar degree (Fig. 2K). Importantly, an additive effect on transmigration was not observed in emerin+cPLA2 RNAi cells, which suggests they are in the same pathway (Figs 2K and 4A).

To reinforce the findings from our migration studies, we subsequently measured nuclear stiffness. To accomplish this, we utilized a previously described approach that involves sandwiching cells or isolated nuclei between two polyacrylamide (PA) gels of known stiffness (1 kPa). By taking the ratio of the height and width, we were able to measure ‘stiffness’ (Liu et al., 2015). When using intact cells, neither emerin RNAi nor emerin OE led to significant changes in stiffness (Fig. 3A-C). However, two emerin mutants, the Phe240His-Frame Shift (Phe240His-FS; ΔINM) and the Q133H substitution, significantly increased cell stiffness (Fig. 3C). As previously described, the Phe240His-FS mutation impairs the ability of emerin to localize to the inner nuclear membrane (INM) (Pfaff et al., 2016). The Q133H mutation is sufficient to cause Emery–Dreifuss muscular dystrophy (EDMD), and disrupts interactions between emerin and HDAC3, the pointed end of filamentous-actin (F-actin) and the inner nuclear membrane protein MAN1 (also known as LEMD3) (Berk et al., 2013). By binding the pointed end, emerin is thought to stabilize F-actin near the INM (Holaska et al., 2004). To measure nuclear stiffness more directly, we disrupted cortical actin using latrunculin-A (Lat-A; 500 nM). By using this approach, emerin RNAi led to a significant increase in stiffness (Fig. 3D). Although lamin A OE increased stiffness, emerin OE led to a significant decrease in stiffness (Fig. 3E). Because of its interactions with F-actin, we wondered whether F-actin is important for emerin function and, therefore, turned to using isolated nuclei. F-actin in the nucleus has numerous functions, including in DNA repair (Belin and Mullins, 2013). By using isolated nuclei, we found that both emerin and lamin A OE increased stiffness (Fig. 3F). As demonstrated by emerin ΔINM, this effect is dependent on emerin being localized to the INM (Fig. 3F). Changes in the nuclear aspect ratio, location, migration and leader bleb area were similarly dependent on emerin being localized to the INM (Fig. S2A-I). Isolated nuclei with emerin Q133H were stiffer – albeit to a lesser degree – when compared to emerin WT (Fig. 3F). Therefore, the Q133H mutation appears to not completely block nuclear stiffening. Likewise, nuclear aspect ratio, location, migration and leader bleb area were between that of cells

Journal of Cell Science (2022) 135, jcs259493. doi:10.1242/jcs.259493

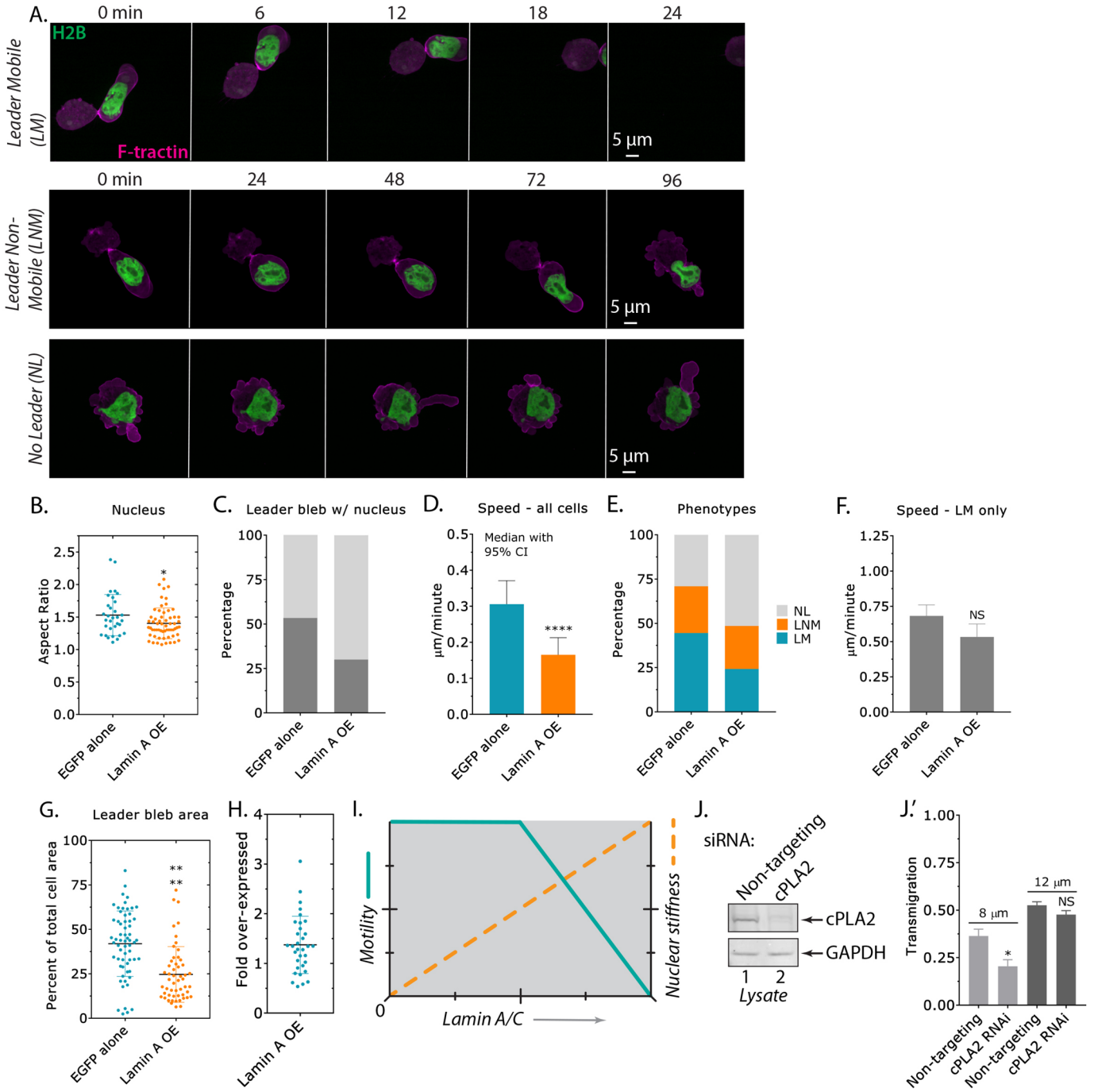

Fig. 1. Fast amoeboid migration is inhibited by high levels of lamin A. (A) Time-lapse imaging of melanoma A375-M2 cells confined down to ∼3 µm, and transiently transfected with H2B-mEmerald and F-tractin-FusionRed to mark nuclei and F-actin, respectively. (B) Nuclear aspect ratio for cells expressing EGFP alone or lamin A-mEmerald (mean±s.d.; two-tailed Student's *t*-test). (C) The percentage of cells with leader blebs containing the nucleus (indicated in dark grey) for EGFP alone or lamin A-mEmerald. (D) Instantaneous speed measured for all cells expressing EGFP alone or lamin A-mEmerald (median±95% c.i.; two-tailed Student's *t*-test). (E) NL, LNM and LM phenotypes in percent for cells expressing EGFP alone or lamin A-mEmerald. Statistical significance was determined using a Chi-squared test (χ^2=1.16×10^{-8}). (F) Instantaneous speed measured for leader mobile (LM) cells expressing EGFP alone or lamin A-mEmerald (mean±s.e.m.; two-tailed Student's *t*-test). (G) Leader bleb area (calculated as the percentage of total cell area) for cells expressing EGFP alone or lamin A-mEmerald (mean ±s.d.; two-tailed Student's *t*-test). (H) Immunofluorescence was used to conduct a cell-by-cell analysis of lamin A overexpression (OE; mean±s.d.). (I) Motility and nuclear stiffness as a function of increasing levels of lamin A (conceptualized). (J) Western blot, confirming RNAi of cPLA2 in A375-M2 cells. (J′) Transmigration of cPLA2 RNAi cells through 8 or 12 µm pores. Statistical significance was determined by a multiple-comparison post hoc test. All data are representative of at least three independent experiments. *P≤0.05, ****P≤0.0001; NS, not significant.

expressing EGFP alone and emerin WT (Fig. S3A-H). The stiffness of isolated nuclei was unaffected by treatment with Lat-A, however, whether isolated nuclei are sensitive to actin monomer-sequestering drugs is unknown (Fig. 3G). In contrast, de-condensation of chromatin in response to the histone deacetylase (HDAC) inhibitor Trichostatin-A (3 µM) significantly decreased the stiffness of isolated nuclei (Fig. 3G). In parallel flow cytometry studies, the total levels of F-actin in cells were found to be unaffected by

Journal of Cell Science

Journal of Cell Science (2022) 135, jcs259493. doi:10.1242/jcs.259493

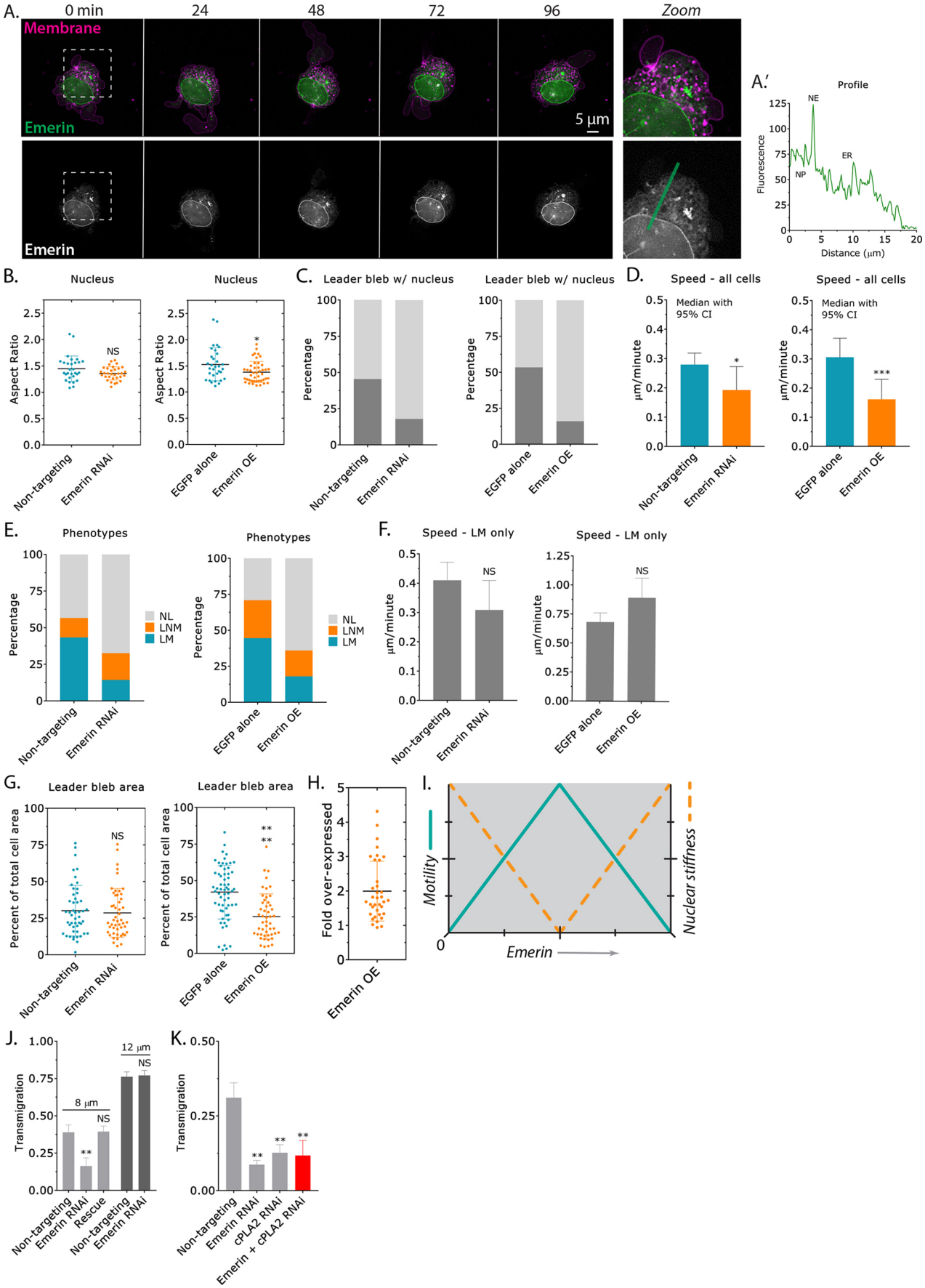

Fig. 2. See next page for legend.

Journal of Cell Science (2022) 135, jcs259493. doi:10.1242/jcs.259493

Fig. 2. Fast amoeboid migration is inhibited by up- or downregulation of emerin. (A) Time-lapse imaging of an A375-M2 cell confined down to ∼3 µm, transiently transfected with emerin-EGFP and stained with membrane dye. Panels on the right (Zoom) show emerin predominantly located at the nuclear envelope and ER. (A′) Line scan (green line) highlighting the enrichment of emerin at the nuclear envelope (NE) and endoplasmic reticulum (ER). NP, nucleoplasm. (B) Nuclear aspect ratio of emerin siRNA-treated cells or cells treated with non-targeting control siRNA (left panel) and in cells overexpressing emerin (OE) or EGFP alone (right panel) (mean±s.d.; two-tailed Student's *t*-test). (C) Percentage of cells with leader blebs containing the nucleus (indicated in dark grey) for emerin RNAi (left) and overexpressing (OE; right) cells. (D) Instantaneous speed measured for cells transfected with non-targeting control siRNA or siRNA against emerin (left, panel) and for cells expressing EGFP alone or emerin (right panel) (median±95% c.i.; two-tailed Student's *t*-test). (E) NL, LNM and LM phenotypes in percent for cells transfected with non-targeting control siRNA or siRNA against emerin (left panel) and for cells expressing EGFP alone or emerin (right panel). Statistical significance was determined using Chi-squared (χ^2) test (emerin RNAi; $\chi^2=2.97\times10^{-7}$, overexpression; $\chi^2=7.69\times10^{-14}$). (F) Instantaneous speeds measured for leader mobile (LM) cells transfected with non-targeting control siRNA or siRNA against emerin (left panel) and for cells expressing EGFP alone or emerin (right panel) (mean±s.e.m.; two-tailed Student's *t*-test). (G) Leader bleb area (calculated as the total cell area in percent) for cells transfected with non-targeting control siRNA or siRNA against emerin (left panel) and for cells expressing EGFP alone or emerin (right panel) (mean ±s.d.; two-tailed Student's *t*-test). (H) Immunofluorescence was used to conduct a cell-by-cell analysis of emerin overexpression (OE; mean±s.d.). (I) Motility and nuclear stiffness as a function of increasing emerin levels (conceptualized). (J) Transmigration (as a percentage) of cells transfected with non-targeting control siRNA or siRNA against emerin through 8 or 12 µm pores. An RNAi-resistant version of emerin-EGFP was used in rescue experiments. Statistical significance was determined by a multiple-comparison post hoc test. (K) Transmigration (as a percentage) of cells expressing non-targeting control siRNA, siRNA against emerin, siRNA against cPLA2 or siRNA against emerin+cPLA2 through 8 µm pores. Statistical significance was determined by a multiple-comparison post hoc test. All data are representative of at least three independent experiments. *$P\leq0.05$, **$P\leq0.01$, ***$P\leq0.001$ and ****$P\leq0.0001$. NS, not significant.

emerin RNAi or OE (WT, ΔINM, Q133H and Y74F/Y95F; Fig. S5A,B). Therefore, nuclear stiffening upon emerin OE requires F-actin.

It has been demonstrated that Src-mediated phosphorylation of emerin at residues Y74 and Y95 is required for nuclei to stiffen in response to force (Guilluy et al., 2014). Therefore, we wondered whether decreased fast amoeboid migration in emerin OE cells, which correlates with increased nuclear stiffness, is dependent on its phosphorylation (Fig. 4A). Cells transfected with the emerin double-mutant Y74F/Y95F were found to have rounder nuclei, whereas the location of the nucleus was unaffected (Fig. 4B-D). Relative to emerin WT, cells with emerin (Y74F/Y95F) were significantly faster (Fig. 4E). Moreover, a larger fraction of cells with emerin (Y74F/Y95F) were mobile (Fig. 4F,G). Whereas emerin WT increased the stiffness of isolated nuclei, it was unaffected by emerin (Y74F/Y95F) (Fig. 4H,I), which is consistent with a role for nuclear stiffness in regulating fast amoeboid migration. Moreover, treatment with the Src family kinase (SFK) inhibitor Dasatinib (500 nM) significantly reduced the stiffness of isolated nuclei (Fig. 4J). In emerin (Y74F/Y95F) OE cells, the leader bleb area was between that of cells expressing EGFP alone and emerin WT (Fig. 4J and Movie 5). Emerin (Y74F/Y95F) was found to be ∼2 fold overexpressed in transfected cells, as measured by IF (Fig. 2H). For cells overexpressing (OE) EGFP alone, emerin WT or Y74F/Y95F, F-actin and myosin were predominantly cortical in their localization (Fig. S4A-C). Accordingly, the inhibition of fast amoeboid (leader bleb-based) migration and increased nuclear stiffness by emerin OE required its phosphorylation (Fig. 4L,M). Notably, the viability of cells after emerin RNAi and overexpression (OE) were similar (Fig. S5C,D).

Based on our data, we predicted that high levels of Src activity inhibit fast amoeboid migration through the phosphorylation of emerin (Fig. 4A). Therefore, we set out to determine the level of Src activity in confined cells. To accomplish this, we used a previously described fluorescence resonance energy transfer (FRET)-based biosensor of Src activity (Ouyang et al., 2008). Between its N- and C-termini this sensor has a donor (ECFP), an SH2 domain, a linker, a Src substrate peptide, an acceptor (YPet) and a membrane anchor. By using freshly plated (spherical) cells, we confirmed that the emission ratio (i.e. acceptor/donor) of the sensor can be lowered by treatment with the SFK inhibitor Dasatinib (0.5 µM; 10 min) (Fig. 5A). Relative to freshly plated (spherical) cells, the emission ratio was significantly lower in cells confined down to ∼3 µm (Fig. 5B). As an additional measure of Src activity, we calculated FRET efficiencies by using the acceptor photobleaching method (Verveer et al., 2006). For freshly plated (spherical) cells, we calculated an average FRET efficiency of 17.29±0.072% (±s.d.) (Fig. 5C,D). For cells confined down to 3 µm, we calculated an average FRET efficiency of 8.457±0.032% (±s.d.), which is indicative of a decrease in Src activity in confined cells (Fig. 5C,D). Therefore, by downregulating Src activity, melanoma cells appear to be primed for fast amoeboid (leader bleb-based) migration.

DISCUSSION

As the largest organelle, the nucleus is subjected to an array of forces during cell migration. In confined environments, which may compress the nucleus, tension at the nuclear membrane with intracellular Ca^{2+} was shown to activate cPLA2 (Lomakin et al., 2020; Venturini et al., 2020). At the nuclear membrane, cPLA2 liberates arachidonic acid, thereby elevating actomyosin contractility (Gong et al., 1992). Importantly, we confirmed using RNAi that cells require cPLA2 for transmigration through confining pores. Accordingly, the mechanical properties of the nucleus are likely to be a major regulator of fast amoeboid (leader bleb-based) migration.

In melanoma cells, we observed that nuclei underwent rapid changes in shape and moved into leader blebs during fast amoeboid migration. By upregulating lamin A, a key component of the lamin nuclear skeleton, we could suppress some of these shape changes and the movement of nuclei into leader blebs (Ungricht and Kutay, 2017). Importantly, upregulating lamin A inhibited the transition to fast amoeboid migration, correlating with a decrease in leader bleb area. As lamin A levels and nuclear stiffness correlate, these results suggest that the mechanical properties of the nucleus regulate fast amoeboid migration. It is noteworthy that downregulation of lamin A had a less pronounced effect. This is not surprising, as many solid tumors already have low levels of lamin A (Dubik and Mai, 2020).

Subsequently, we determined the role of the INM protein emerin in regulating fast amoeboid (leader bleb-based) migration. Although loss-of-function mutations of emerin are well known in EDMD, the role of emerin in regulating other cell biological processes is less well understood (Nagano et al., 1996). The discovery that emerin is key to nuclear stiffening in response to force, implies that emerin is crucially important in diverse cell types. In motile cells, emerin might regulate the passage of cells through confined environments and protect the genome by preventing nuclear rupture (Denais et al., 2016; Raab et al., 2016). Accordingly, perturbation of emerin function may prevent or abate cancer metastasis. In melanoma cells,

Journal of Cell Science (2022) 135, jcs259493. doi:10.1242/jcs.259493

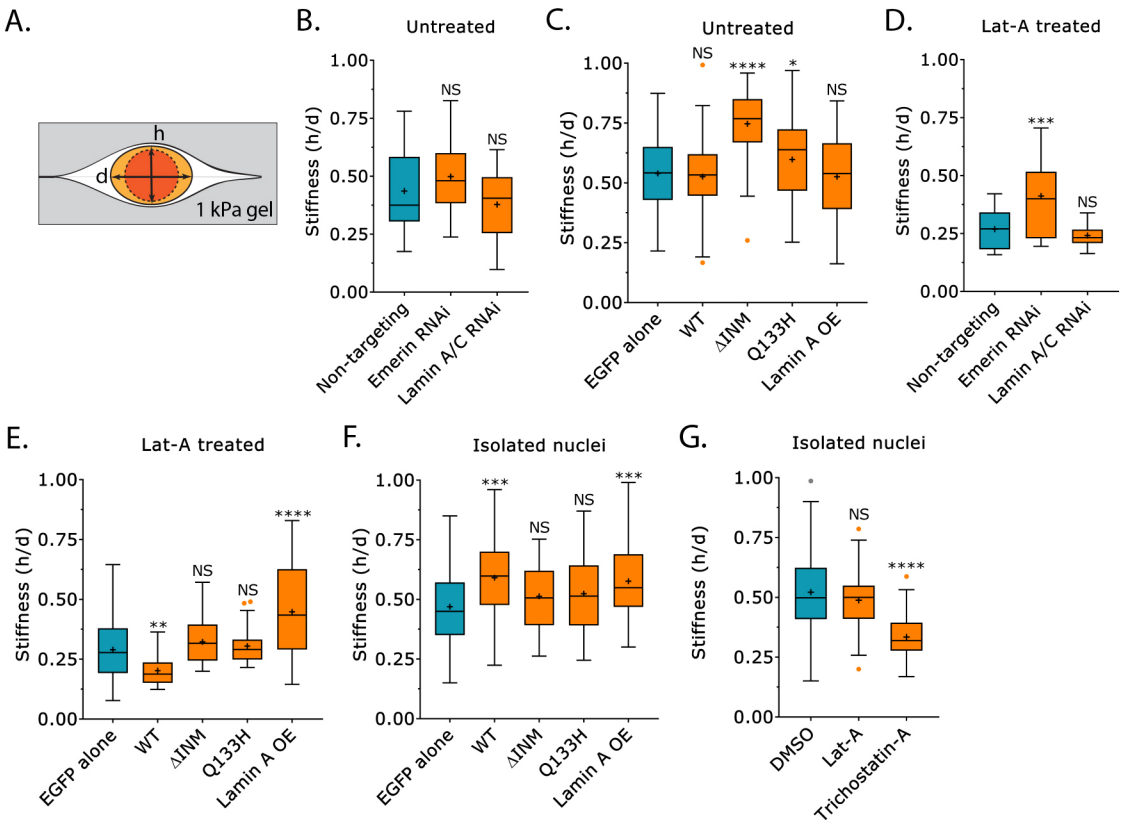

Fig. 3. Nuclear stiffness is increased by up- or downregulation of emerin. (A) Schematic of the gel sandwich approach to measure stiffness. (B) Stiffness as height divided by diameter (*h*/*d*) for intact (untreated) cells after RNAi using a non-targeting control siRNA (53 cells), siRNA against emerin (49 cells) or siRNA against lamin A/C (46 cells). (C) Stiffness (*h*/*d*) for intact (untreated) cells overexpressing (OE) EGFP alone (185 cells), emerin WT (70 cells), ΔINM (67 cells), Q133H (106 cells) or lamin A (51 cells). (D) Stiffness (*h*/*d*) for latrunculin-A (Lat-A)-treated (500 nM) cells after RNAi using a non-targeting control siRNA (48 cells), siRNA against emerin (54 cells) or siRNA against lamin A/C (48 cells). (E) Stiffness (*h*/*d*) for Lat-A-treated(500 nM) cells overexpressing (OE) EGFP alone (105 cells), emerin WT (47 cells), ΔINM (49 cells), Q133H (67 cells) or lamin A (46 cells). (F) Stiffness (*h*/*d*) for isolated nuclei (post cell fractionation) after overexpressing (OE) EGFP alone (105 nuclei), emerin WT (45 nuclei), ΔINM (45 nuclei), Q133H (41 nuclei) or lamin A (57 nuclei). (G) Stiffness (*h*/*d*) for isolated nuclei (post cell fractionation) after treatment with DMSO (166 nuclei), Lat-A (500 nM; 41 nuclei) or Trichostatin-A (3 µM; 90 nuclei). Statistical significance was determined by multiple-comparison post hoc tests. All data are representative of at least three independent experiments. *$P\leq0.05$, **$P\leq0.01$, ***$P\leq0.001$ and ****$P\leq0.0001$. NS, not significant. For box plots, + and horizontal lines denote the mean and median, respectively; orange dots in C, E and G indicate outliers.

we determined the role of emerin in regulating fast amoeboid migration. As in other cell types, emerin in melanoma cells predominantly localized to the nuclear envelope and ER. Strikingly, up- or downregulation of emerin, led to rounder nuclei that were less often positioned in leader blebs. Cells in which emerin had been up- or downregulated were also less often motile, correlating with a decrease in the leader bleb area. Together, these results suggested that melanoma cells require intermediate or endogenous levels of emerin for fast amoeboid migration. In agreement with the concept that emerin regulates the activity of cPLA2 through changes in nuclear deformability, RNAi of emerin, cPLA2 and emerin+cPLA2 led to similar rates of transmigration through confining pores. However, as the nuclear lamina is known to play a role in chromatin organization, we cannot rule out the possibility that multiple genes are de-regulated as a result of changes in emerin activity.

Our results suggested that emerin may regulate fast amoeboid migration through changes in nuclear mechanics. Therefore, by measuring compressibility, we determined the stiffnesses of cells and isolated nuclei. By using intact cells, we were unable to detect any differences in stiffness after up- or downregulation of emerin. However, after removal of cortical actin with Lat-A, we could detect an increase in stiffness after downregulation of emerin. Surprisingly, in Lat-A-treated cells, the stiffness of cells in which emerin was upregulated was reduced. Therefore, we wondered whether F-actin is important for emerin function. Notably, emerin has been shown to interact with the pointed end of F-actin (Holaska et al., 2004). Indeed, using isolated nuclei from cells in which F-actin has not been perturbed, we could detect that emerin upregulation increased stiffness. Moreover, this effect was dependent on emerin being localized to the INM. Interestingly, the stiffness of isolated nuclei containing the Q133H mutant of emerin, which is found in EDMD patients, was between that of cells expressing control (EGFP alone) and emerin WT (Berk et al., 2013). The Q133H mutation is known to disrupt interactions between emerin, HDAC3, F-actin and MAN1 (Berk et al., 2013). This suggested to us that F-actin in the nucleus regulates its stiffness, but we could not detect a significant decrease in stiffness when treating nuclei with Lat-A. However, actin monomer sequestering drugs might not be sufficient to disassemble F-actin in the nucleus. In contrast, chromatin de-condensation led to a significant reduction in the stiffness of isolated nuclei. In agreement with other labs, our data suggest that changes in chromatin structure are more likely to regulate nuclear stiffness (Nava et al., 2020).

In response to force, Src phosphorylates emerin at residues Y74 and Y95, thereby increasing nuclear stiffness (Guilluy et al., 2014). Therefore, we wondered whether inhibition of fast amoeboid

Journal of Cell Science (2022) 135, jcs259493. doi:10.1242/jcs.259493

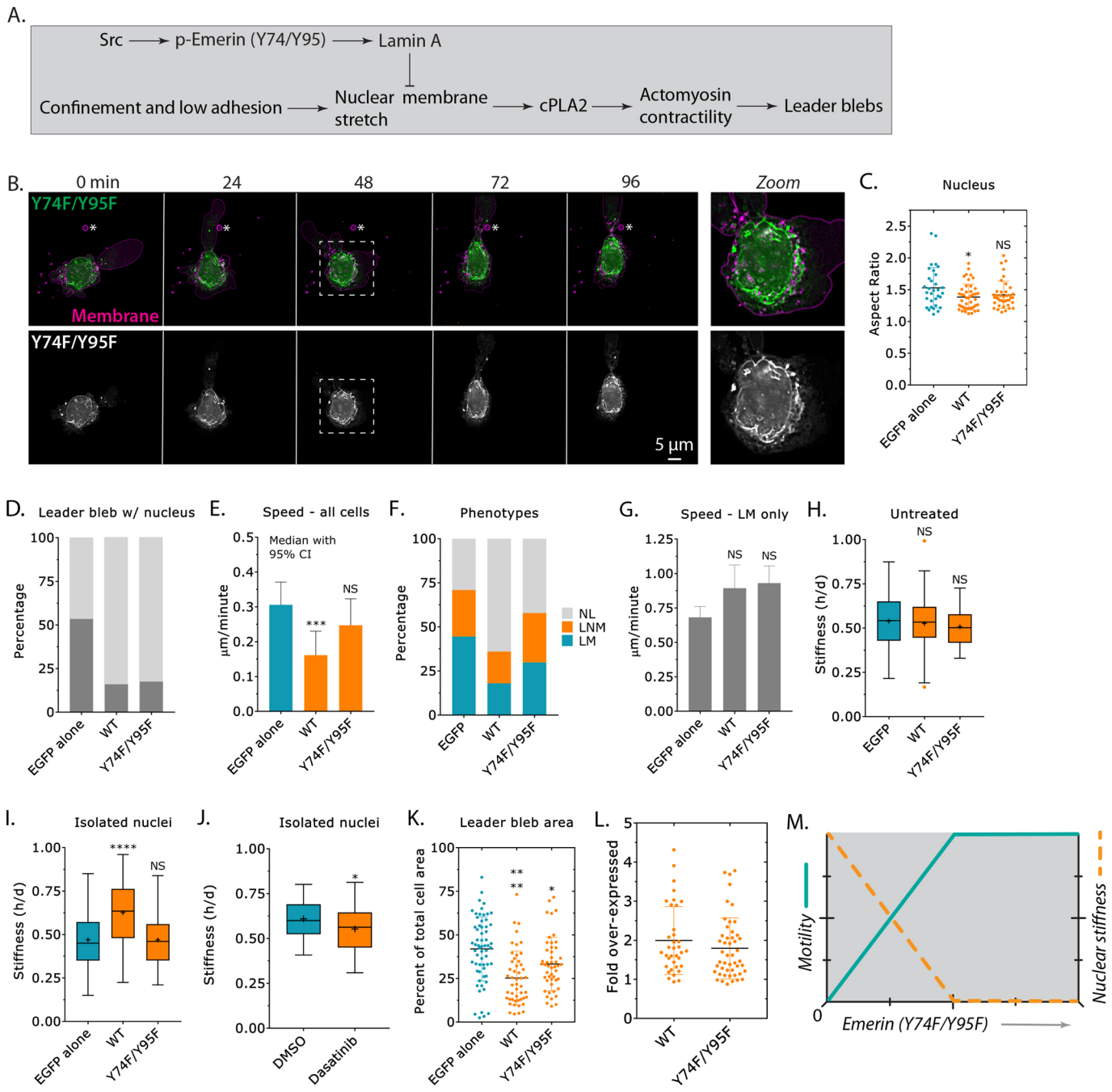

Fig. 4. Src mediated phosphorylation of emerin at residues Y74 and Y95 inhibits fast amoeboid migration. (A) Schematic of the investigated pathway. (B) Time-lapse imaging of a melanoma A375-M2 cell that was confined down to ∼3 µm, transiently transfected with emerin-EGFP (Y74F/Y95F) and stained with membrane dye. Panels on the right (Zoom) show emerin-EGFP (Y74F/Y95F) predominantly located at the nuclear envelope and ER. (C) Nuclear aspect ratio of cells overexpressing EGFP alone, emerin WT or emerin Y74F/Y95F (mean±s.d.; multiple-comparison post hoc test). (D) The percentage of cells with leader blebs containing the nucleus (indicated in dark grey) for EGFP alone, emerin WT or Y74F/Y95F. (E) Instantaneous speeds measured for all cells, overexpressing EGFP alone, emerin WT or emerin Y74F/Y95F (median±95% c.i.; multiple-comparison post hoc test). (F) NL, LNM and LM phenotypes in percent for cells overexpressing EGFP alone, emerin WT or Y74F/Y95F. Statistical significance was determined using a Chi-squared test (EGFP alone vs Y74F/Y95F; χ^2=0.000104). (G) Instantaneous speeds measured for leader mobile (LM) cells overexpressing EGFP alone, emerin WT or Y74F/Y95F (mean±s.e.m.; multiple-comparison post hoc test). (H) Stiffness as height divided by diameter (*h*/*d*) of intact (untreated) cells overexpressing EGFP alone (185 cells), emerin WT (70 cells) or emerin Y74F/Y95F (57 cells). Statistical significance was determined by a multiple-comparison post hoc test. For comparison, data for EGFP alone and emerin WT were reproduced from Fig. 3C. (I) Stiffness (*h*/*d*) of isolated nuclei (post cell fractionation) after overexpressing EGFP alone (81 nuclei), emerin WT (45 nuclei) or emerin Y74F/Y95F (42 nuclei). Statistical significance was determined by a multiple-comparison post hoc test. For comparison, data for EGFP alone and emerin WT were reproduced from Fig. 3F. (J) Stiffness (*h*/*d*) of isolated nuclei (post cell fractionation) after treatment with DMSO (52 nuclei) or Dasatinib (56 nuclei; 500 nM). Statistical significance was determined by a two-tailed Student's *t*-test. (K) Leader bleb area (calculated as the total cell area in percent) for cells overexpressing EGFP alone, emerin WT or emerin Y95F/Y74F (mean±s.d.; multiple-comparison post hoc test). (L) Immunofluorescence was used to conduct a cell-by-cell analysis of emerin WT and emerin Y74F/Y95F overexpression (mean±s.d.). (M) Motility and nuclear stiffness as a function of increasing levels of emerin Y74F/Y95F (conceptualized). All data are representative of at least three independent experiments. *P≤0.05, ***P≤0.001 and ****P≤0.0001. NS, not significant. For box plots, + and horizontal lines denote the mean and median, respectively; orange dots in H indicate outliers.

Journal of Cell Science (2022) 135, jcs259493. doi:10.1242/jcs.259493

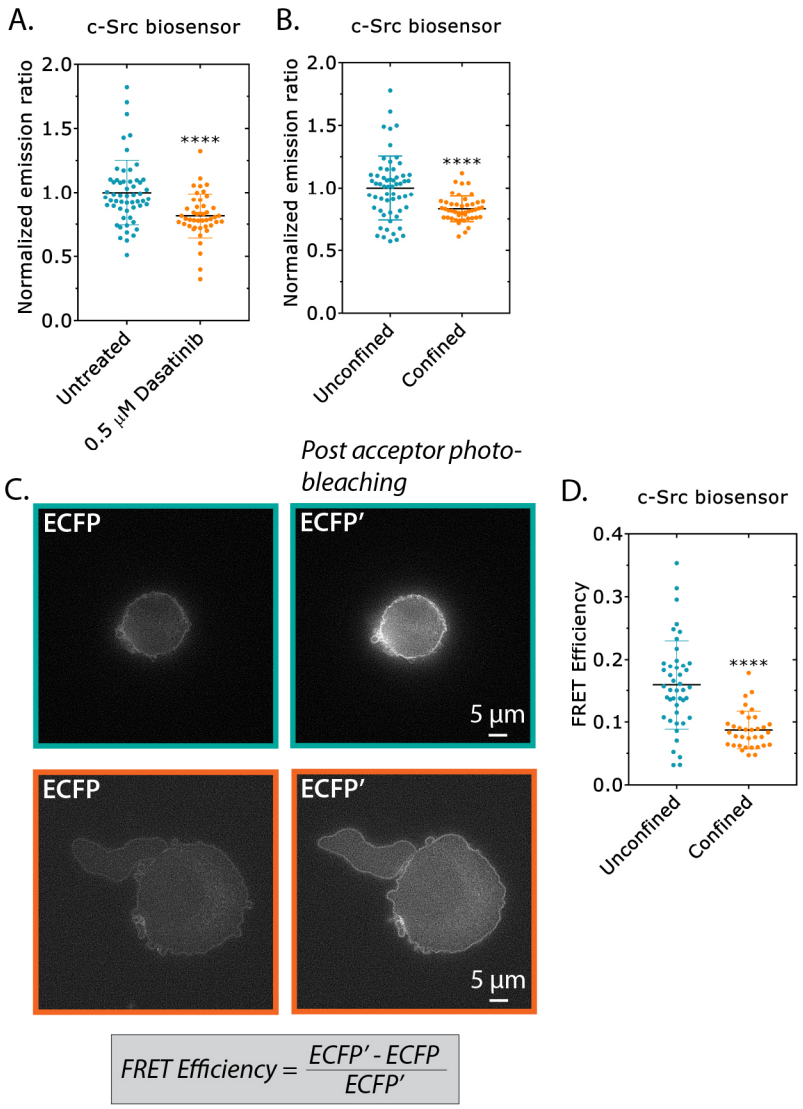

Fig. 5. Confined cells have low levels of Src activity. (A) Normalized emission ratio (acceptor/donor) for freshly plated (spherical) cells treated with the SFK inhibitor Dasatinib (0.5 µM; 10 min) (mean±s.d.; two-tailed Student's *t*-test). (B) Normalized emission ratio of ECFP (acceptor/donor) for freshly plated (spherical) cells and that have been confined down to 3 µm (mean±s.d.; two-tailed Student's *t*-test). (C) Top: ECFP (FRET donor) before and after acceptor photobleaching in a freshly plated (spherical) cell. Bottom: ECFP (FRET donor) before and after acceptor photobleaching in a cell that has been confined down to ∼3 µm. The equation used for calculating FRET efficiencies is shown below. (D) FRET efficiencies for freshly plated (spherical) cells and that have been confined down to ∼3 µm (mean±s.d.; two-tailed Student's *t*-test). All data are representative of at least three independent experiments. ****$P \leq 0.0001$.

migration by emerin OE is dependent on its phosphorylation. Indeed, we found that, in cells with emerin (Y74F/Y95F), nuclei appeared more dynamic, as assessed by analyzing the nuclear aspect ratio and localization. Moreover, cells were more often mobile, which correlated with softer isolated nuclei. Additionally, treating isolated nuclei with the SFK inhibitor Dasatinib led to a significant decrease in stiffness. Thus, high Src activity should inhibit fast amoeboid (leader bleb-based) migration. Accordingly, we determined the levels of Src activity in confined cells. Strikingly, we found that, relative to freshly plated (spherical) cells, confined cells had lower levels of Src activity. These data are consistent with previous work from our lab, showing that fast amoeboid (leader bleb-based) migration is inhibited by high Src activity (Logue et al., 2018; Ullo and Logue, 2018). It appears that, when upregulated, a significant fraction of emerin becomes phosphorylated, even when Src activity is relatively low. By using isolated nuclei, it has been reported that pulling anti-nesprin-1-coated beads with magnetic tweezers activated Src; therefore, environments that require migrating cells to repeatedly pull on their nucleus – e.g. confining pores – may activate Src (Guilluy et al., 2014; McGregor et al., 2016). To the best of our knowledge, it is unknown how pulling on nesprin-1 activates Src near the nuclear envelope. Nesprin-1 connects F-actin in the cytoplasm to the nuclear lamina (Lombardi et al., 2011) but, as actin is predominantly cortical in fast amoeboid cells, the nucleus may not be subjected to strong pulling forces through nesprin-1.

Collectively, our data demonstrate that the precise calibration of emerin activity is required for fast amoeboid (leader bleb-based) migration. Thus, the perturbation of emerin function may abate or prevent cancer metastasis.

MATERIALS AND METHODS

Cell culture

A375-M2 cells (CRL-3223) were obtained from the American Type Culture Collection (ATCC; Manassas, VA). Cells were cultured in high-glucose DMEM (cat no. 10569010; Thermo Fisher, Carlsbad, CA) supplemented with 10% FBS (cat no. 12106C; Sigma Aldrich, St Louis, MO), antibiotic-antimycotic (cat no. 15240112; Thermo Fisher) and 20 mM HEPES at pH 7.4 for up to 30 passages. Cells were plated at a density of 750,000 cells per well in a six-well plate the day of transfection.

Pharmacological treatments

Latrunculin-A (Lat-A; cat no. 3973), Trichostatin-A (cat no. 1406) and Dasatinib (cat no. 6793) were purchased from Tocris Bioscience (Bristol, UK). All drugs were dissolved in DMSO (Sigma Aldrich). Cells were treated with Lat-A for 15 min, Trichostatin-A overnight or Dasatinib for

Journal of Cell Science (2022) 135, jcs259493. doi:10.1242/jcs.259493

30 min. Prior to measurements of nuclear stiffness, polyacrylamide gels were incubated for 30 min in buffer S (20 mM HEPES at pH 7.8, 25 mM KCl, 5 mM $MgCl_2$, 0.25 M sucrose and 1 mM ATP) with DMSO or drug.

Plasmids

F-tractin-FusionRed has been previously described (Logue et al., 2015). H2B-FusionRed was purchased from Evrogen (Moscow, Russia). mEmerald-LaminA-C-18 (Addgene plasmid no. 54138) and mEmerald-Nucleus-7 (Addgene plasmid no. 54206) were gifts from Michael Davidson (Florida State University). Emerin pEGFP-N2 (588; Addgene plasmid no. 61985) and Emerin pEGFP-C1 (637; Addgene plasmid no. 61993) were gifts from Eric Schirmer (University of Edinburgh). Kras-Src FRET biosensor (Addgene plasmid no. 78302) was a gift from Yingxiao Wang (University of Illinois). 1 µg of plasmid was used to transfect 750,000 cells in each well of a six-well plate using Lipofectamine 2000 (5 µl; Thermo Fisher) in OptiMEM (400 µl; Thermo Fisher). After 30 min at room temperature, plasmid in Lipofectamine 2000/OptiMEM was then incubated with cells in complete medium (2 ml) overnight.

Mutagenesis

Emerin mutants were generated using the QuikChange II XL Site-Directed Mutagenesis Kit (Agilent Technologies; Santa Clara, CA) according to the manufacturer's protocol. The following forward primers were used for PCR:

Emerin RNAi resistant: 5′-CTCCCTGGACCTGTCTTATTATCCTA-CTTCC-3′, Phe240His-FS (ΔINM): 5′-GTGATCGTCCTCCATTTACCA-CTTC-3′, Q133H: 5′-GCYTTTCCATCACCATGTGCATGATGACG-3′, Y74F: 5′-GGGATGCAGATATGTTTGATCTTCCCAAGAAAGAGGA-3′, Y95F: 5′-GGCTACAATGACGACTACTTTGAAGAGAGCTACTTC-3′.

RNAi-resistant emerin yields a single (silent; C→T) mutation centrally located within the LNA target sequence (5′-GACCTGTCCTATTATCCTA-3′). All clones were verified by sequencing using a commercially available resource (Genewiz, South Plainfield, NJ).

LNAs

Non-targeting control small interference RNA (siRNA) (cat no. 4390844), lamin A/C (cat no. 4390824; s8221) and emerin (cat no. 4392420; s225840) Locked Nucleic Acids (LNAs) were purchased from Thermo Fisher. All LNA transfections were performed using RNAiMAX (5 µl; Thermo Fisher) and OptiMEM (400 µl; Thermo Fisher). Briefly, cells were trypsinized and seeded in six-well plates at 750,000 cells per well in complete medium. After cells adhered (∼1 h), LNAs in RNAiMAX/OptiMEM were added to cells in complete medium (2 ml) at a final concentration of 50 nM. Cells were incubated with LNAs for as long as 5 days.

Western blotting

Whole-cell lysates were prepared by scraping cells into ice cold RIPA buffer (50 mM HEPES pH 7.4, 150 mM NaCl, 5 mM EDTA, 0.1% SDS, 0.5% deoxycholate and 1% Triton X-100) containing protease and phosphatase inhibitors (Roche, Switzerland). Before loading onto 4–12% NuPAGE Bis-Tris gradient gels (Thermo Fisher), DNA was sheared by sonication and samples were boiled for 10 min in loading buffer. Following SDS-PAGE, proteins in gels were transferred to nitrocellulose membranes and subsequently immobilized for 15 min by 0.1% glutaraldehyde (Electron Microscopy Sciences; Hatfield, PA). After blocking in Tris-buffered saline containing 0.1% Tween 20 (TBS-T) and 1% BSA, primary antibodies against lamin A/C (cat no. 2032; Cell Signaling Technology) or emerin (cat no. 30853; Cell Signaling Technology) were incubated with membranes overnight at 4°C. Bands were then resolved with horseradish peroxidase (HRP)-conjugated secondary antibodies and a C-Digit imager (LI-COR Biosciences, Lincoln, NE). GAPDH (cat no. 97166; Cell Signaling Technology) was used to confirm equal loading.

Immunofluorescence (IF)

After washing with HEPES-buffered saline (HBS), cells in six-well glass-bottom plates (Cellvis) were fixed with 4% paraformaldehyde (Electron Microscopy Sciences) in HBS for 20 min at room temperature. Blocking, permeabilization, antibody incubation and washing were done in HBS with 1% BSA, 1% fish gelatin, 0.1% Triton X-100 and 5 mM EDTA. Then, a 1:250 dilution of lamin A/C (cat no. 2032; Cell Signaling Technology) or emerin (cat no. 30853; Cell Signaling Technology) antibody was incubated with cells overnight at 4°C. After extensive washing, a 1:400 dilution of Alexa Fluor 568-conjugated anti-rabbit secondary antibody (cat no. A-11036; Thermo Fisher) was incubated with cells for 2 h at room temperature. Cells were then incubated with a 1:1000 dilution of DAPI (cat no. D1306; Thermo Fisher). Cells were again extensively washed and then imaged in HBS. Cell-by-cell analyses of overexpression levels were conducted by comparing fluorescence intensities between transfected and non-transfected cells. Transfected cells were identified by using the fluorescent protein tag.

Microscopy

High-resolution imaging was performed using a General Electric (Boston, MA) DeltaVision Elite imaging system mounted on an Olympus (Japan) IX71 stand with a computerized stage, Ultimate Focus; environment chamber (heat, CO_2 and humidifier); ultrafast solid-state illumination with excitation/emission filter sets for DAPI, CFP, GFP, YFP and Cy5 critical illumination; Olympus PlanApo N 60×/1.42 NA DIC (oil) objective; Photometrics (Tucson, AZ) CoolSNAP HQ2 camera; proprietary constrained iterative deconvolution and vibration isolation table.

Confinement

This protocol has been described in detail elsewhere (https://protocolexchange.researchsquare.com/article/nprot-6585/v1). Briefly, polydimethylsiloxane (PDMS; 184 SYLGARD) was purchased from Krayden (Westminster, CO). Overnight, 2 ml was cured at 37°C in each well of a six-well glass bottom plate (Cellvis, Mountain View, CA). Using a biopsy punch (cat no. 504535; World Precision Instruments, Sarasota, FL), an 8 mm hole was cut and 3 ml of serum-free medium containing 1% BSA was added to each well and incubated overnight at 37°C. After medium removal, 200 µl of complete medium containing trypsinized cells (250,000 to 1 million) and 2 µl of beads (3.11 µm; Bangs Laboratories, Fishers, IN) were then pipetted into the round opening. The vacuum created by briefly lifting one side of the hole with a 1 ml pipette tip was used to move cells and beads underneath the PDMS. Finally, 3 ml of complete medium was added to each well and cells were recovered for ∼60 min before imaging. Here, complete medium consisted of FluoroBrite (cat no. A1896701; Thermo Fisher) supplemented with 20% FBS (cat no. 12106C; Sigma Aldrich), antibiotic-antimycotic (cat no. 15240112; Thermo Fisher), and 20 mM HEPES at pH 7.4.

Leader blebs containing the cell nucleus

A thematic analysis of leader blebs and the nucleus was done for every cell by eye, i.e. when the nucleus moved into the leader bleb from the cell body and remained there for at least three consecutive frames, the cell was classified as having a 'leader bleb containing the nucleus'.

Classification of leader mobile, leader non-mobile and no leader cells

For classification, freshly confined cells were imaged every 8 min for 5 h. Cells were classified by eye as either leader mobile (LM; cells that form leader blebs and are mobile), leader non-mobile (LNM; cells with a leader bleb that persists for at least five consecutive frames but do not move), or no leader (NL; cells that do not form leader blebs and are non-mobile).

Instantaneous speed

Cells were tracked manually using the Fiji (https://fiji.sc/) plugin, MTrackJ, developed by Meijering and colleagues (Gorelik and Gautreau, 2014; Meijering et al., 2012). Instantaneous speeds from manual tracking were determined using the Excel (Microsoft; Redmond, WA) plugin, DiPer, developed by Gorelik and colleagues (Gorelik and Gautreau, 2014; Meijering et al., 2012). To minimize positional errors, cells were tracked every 8 min for 5 h. Brightfield imaging was used to confirm that beads were not obstructing the path of a cell.

Leader bleb area

For leader bleb area, freshly confined cells were imaged every 8 min for 5 h and cells were traced from high-resolution images with the free-hand circle tool in Fiji (https://fiji.sc/). From every frame, the percent of total cell area for leader blebs was calculated in Excel (Microsoft) as the measured leader bleb area divided by the total cell area for the same frame. Measurements were then combined to generate an average for each cell.

Cell stiffness assay

The previously described gel sandwich assay was used with minor modifications (Liu et al., 2015). Six-well glass bottom plates (Cellvis) and 18 mm coverslips were activated using 3-aminopropyltrimethoxysilane (Sigma Aldrich) for 5 min and then for 30 min with 0.5% glutaraldehyde (Electron Microscopy Sciences) in PBS. 1 kPa polyacrylamide gels were made using 2 µl of blue fluorescent beads (200 nm; Thermo Fisher), 18.8 µl of 40% acrylamide solution (cat no. 161-0140; Bio-Rad, Hercules, CA), and 12.5 µl of bis-acrylamide (cat no. 161-0142; Bio-Rad) in 250 µl of PBS. Finally, 2.5 µl of ammonium persulfate (APS; 10% in water) and 0.5 µl of Tetramethylethylenediamine (TEMED) was added before spreading 9 µl drops onto treated glass under coverslips. After polymerizing for 40 min, the coverslip was lifted in PBS, extensively rinsed and incubated overnight in PBS. Before each experiment, the gel attached to the coverslip was placed on a 14 mm diameter, 2 cm high PDMS column for applying a slight pressure to the coverslip with its own weight. Then, both gels were incubated for 30 min in medium (cells) or buffer S (isolated nuclei) before plates were seeded. After placing the bottom gels in plates on the microscope stage, the PDMS column with the top gel was placed over the cells seeded on the bottom gels, confining cells between the two gels (Fig. 3A). After 1 h of adaptation, the cell height was determined with beads by measuring the distance between gels. The cell diameter was measured using a far-red plasma membrane dye (cat no. C10046; Thermo Fisher). Stiffness was defined as height (h) divided by diameter (d). When drugs were used, gels were first incubated with drug in medium for 30 min before each experiment.

Nucleus isolation

The protocol for isolating nuclei has been previously described (Guilluy et al., 2014). 24 h prior to nucleus isolation, 750,000 cells per well in a six-well plate were transfected using Lipofectamine 2000 (5 µl; Thermo Fisher) as needed. Cells were lysed in 1 ml of hypotonic buffer (10 mM HEPES, 1 mM KCl, 1 mM $MgCl_2$, 0.5 mM dithiothreitol and protease inhibitors) for 10 min on ice. After cell fragments were detached using a scraper, samples were homogenized using 50 strokes of a tight-fitting Dounce homogenizer and then centrifuged at 700 ***g*** for 10 min at 4°C. Pellets were then washed in hypotonic buffer and centrifuged again. The nuclear pellet was suspended in buffer S (20 mM HEPES at pH 7.8, 25 mM KCl, 5 mM $MgCl_2$, 0.25 M sucrose and 1 mM ATP) and then stained with a far-red fluorescent membrane dye (cat no. C10046; Thermo Fisher). Prior to the cell stiffness assay, the number and purity of nuclei as assessed by size was determined using an automated cell counter (TC20; Bio-Rad, Hercules, CA). For drug treatment, drugs were present throughout the isolation process.

Transmigration

Transmigration assays were performed using polycarbonate filters with 8 or 12 µm pores (Corning; Corning, NY). Prior to the assays, polycarbonate filters were coated with fibronectin (10 µg/ml; Millipore) then air dried for 1 h. 100,000 cells in serum-free medium were seeded in the top chamber while the bottom chamber contained medium with 20% FBS to attract cells. After 24 h, cells from the bottom of the filter were trypsinized and counted using an automated cell counter (TC20; Bio-Rad). The percentage of transmigration was calculated by dividing the number of cells on the bottom by the total and then multiplying by 100.

Src biosensor

FRET efficiencies in unconfined vs confined cells transfected with the Kras-Src FRET biosensor (Addgene plasmid no. 78302; gift from Yingxiao Wang) were calculated using the acceptor photobleaching method (Verveer et al., 2006).

Flow cytometry

For measuring F-actin, trypsinized cells in FACS buffer (PBS with 1% BSA) were fixed using 4% paraformaldehyde (cat no. 15710; Electron Microscopy Sciences) for 20 min at room temperature. After washing, cells were stained with Alexa Fluor 647 conjugated phalloidin (cat no. A22287; Thermo Fisher) and DAPI (Sigma Aldrich) overnight at 4°C. Data were acquired on a FACSCalibur (BD Biosciences; Franklin Lakes, NJ) flow cytometer. Median Fluorescence Intensities (MFIs) were determined using FlowJo (Ashland, OR) software. A detailed description of the flow gating strategy is shown in Fig. S5B.

Statistics

All sample sizes were empirically determined based on saturation. As noted in each figure legend, statistical significance was determined by a two-tailed Student's t-test or one-way ANOVA followed by a multiple-comparison post hoc test. Normality was determined by a D'Agostino–Pearson test in Prism (GraphPad; San Diego, CA). *$P\leq0.05$, **$P\leq0.01$, ***$P\leq0.001$ and ****$P\leq0.0001$. All box plots were plotted using the Tukey method.

Acknowledgements

We thank members of the Logue Lab for insightful discussions. We also thank the administrative staff within the Department of Regenerative and Cancer Cell Biology at the Albany Medical College.

Competing interests

The authors declare no competing or financial interests.

Author contributions

Conceptualization: J.S.L.; Investigation: S.B.L., K.W.V., A.P.C., M.F.U., A.K., J.S.L.; Writing - original draft: J.S.L.; Writing - review & editing: J.S.L., S.B.L.; Visualization: J.S.L.; Supervision: J.S.L.; Project administration: J.S.L.; Funding acquisition: J.S.L.

Funding

This work was supported by start-up funds from the Albany Medical College, a Young Investigator Award from the Melanoma Research Alliance (MRA) (grant no. 688232; https://doi.org/10.48050/pc.gr.91570) and a Cancer Research Scholar Grant from the American Cancer Society (ACS) (grant no. RSG-20-019-01 - CCG) to J.S.L.

Peer review history

The peer review history is available online at https://journals.biologists.com/jcs/article-lookup/doi/10.1242/jcs.259493.

References

Belin, B. J. and Mullins, R. D. (2013). What we talk about when we talk about nuclear actin. *Nucleus* **4**, 291-297. doi:10.4161/nucl.25960

Bergert, M., Erzberger, A., Desai, R. A., Aspalter, I. M., Oates, A. C., Charras, G., Salbreux, G. and Paluch, E. K. (2015). Force transmission during adhesion-independent migration. *Nat. Cell Biol.* **17**, 524-529. doi:10.1038/ncb3134

Berk, J. M., Tifft, K. E. and Wilson, K. L. (2013). The nuclear envelope LEM-domain protein emerin. *Nucleus* **4**, 298-314. doi:10.4161/nucl.25751

Cantelli, G., Orgaz, J. L., Rodriguez-Hernandez, I., Karagiannis, P., Maiques, O., Matias-Guiu, X., Nestle, F. O., Marti, R. M., Karagiannis, S. N. and Sanz-Moreno, V. (2015). TGF-β-induced transcription sustains amoeboid melanoma migration and dissemination. *Curr. Biol.* **25**, 2899-2914. doi:10.1016/j.cub.2015.09.054

Clark, E. A., Golub, T. R., Lander, E. S. and Hynes, R. O. (2000). Genomic analysis of metastasis reveals an essential role for RhoC. *Nature* **406**, 532-535. doi:10.1038/35020106

Denais, C. M., Gilbert, R. M., Isermann, P., McGregor, A. L., te Lindert, M., Weigelin, B., Davidson, P. M., Friedl, P., Wolf, K. and Lammerding, J. (2016). Nuclear envelope rupture and repair during cancer cell migration. *Science* **352**, 353-358. doi:10.1126/science.aad7297

Dubik, N. and Mai, S. (2020). Lamin A/C: function in normal and tumor cells. *Cancers (Basel)* **12**, 3688. doi:10.3390/cancers12123688

Gong, M. C., Fuglsang, A., Alessi, D., Kobayashi, S., Cohen, P., Somlyo, A. V. and Somlyo, A. P. (1992). Arachidonic acid inhibits myosin light chain phosphatase and sensitizes smooth muscle to calcium. *J. Biol. Chem.* **267**, 21492-21498. doi:10.1016/S0021-9258(19)36636-0

Gorelik, R. and Gautreau, A. (2014). Quantitative and unbiased analysis of directional persistence in cell migration. *Nat. Protoc.* **9**, 1931-1943. doi:10.1038/nprot.2014.131

Guilluy, C., Osborne, L. D., Van Landeghem, L., Sharek, L., Superfine, R., Garcia-Mata, R. and Burridge, K. (2014). Isolated nuclei adapt to force and reveal a mechanotransduction pathway in the nucleus. *Nat. Cell Biol.* **16**, 376-381. doi:10.1038/ncb2927

Holaska, J. M., Kowalski, A. K. and Wilson, K. L. (2004). Emerin caps the pointed end of actin filaments: evidence for an actin cortical network at the nuclear inner membrane. *PLoS Biol.* **2**, e231. doi:10.1371/journal.pbio.0020231

Lammerding, J., Fong, L. G., Ji, J. Y., Reue, K., Stewart, C. L., Young, S. G. and Lee, R. T. (2006). Lamins A and C but not lamin B1 regulate nuclear mechanics. *J. Biol. Chem.* **281**, 25768-25780. doi:10.1074/jbc.M513511200

Liu, Y.-J., Le Berre, M., Lautenschlaeger, F., Maiuri, P., Callan-Jones, A., Heuzé, M., Takaki, T., Voituriez, R. and Piel, M. (2015). Confinement and low adhesion induce fast amoeboid migration of slow mesenchymal cells. *Cell* **160**, 659-672. doi:10.1016/j.cell.2015.01.007

Logue, J. S., Cartagena-Rivera, A. X., Baird, M. A., Davidson, M. W., Chadwick, R. S. and Waterman, C. M. (2015). Erk regulation of actin capping and bundling by Eps8 promotes cortex tension and leader bleb-based migration. *eLife* **4**, e08314. doi:10.7554/eLife.08314

Logue, J. S., Cartagena-Rivera, A. X. and Chadwick, R. S. (2018). c-Src activity is differentially required by cancer cell motility modes. *Oncogene* **37**, 2104-2121. doi:10.1038/s41388-017-0071-5

Lomakin, A. J., Cattin, C. J., Cuvelier, D., Alraies, Z., Molina, M., Nader, G. P. F., Srivastava, N., Saez, P. J., Garcia-Arcos, J. M., Zhitnyak, I. Y. et al. (2020). The nucleus acts as a ruler tailoring cell responses to spatial constraints. *Science* **370**, eaba2894. doi:10.1126/science.aba2894

Lombardi, M. L., Jaalouk, D. E., Shanahan, C. M., Burke, B., Roux, K. J. and Lammerding, J. (2011). The interaction between nesprins and sun proteins at the nuclear envelope is critical for force transmission between the nucleus and cytoskeleton. *J. Biol. Chem.* **286**, 26743-26753. doi:10.1074/jbc.M111.233700

Madsen, C. D. and Sahai, E. (2010). Cancer dissemination—lessons from leukocytes. *Dev. Cell* **19**, 13-26. doi:10.1016/j.devcel.2010.06.013

McGregor, A. L., Hsia, C.-R. and Lammerding, J. (2016). Squish and squeeze-the nucleus as a physical barrier during migration in confined environments. *Curr. Opin. Cell Biol.* **40**, 32-40. doi:10.1016/j.ceb.2016.01.011

Meijering, E., Dzyubachyk, O. and Smal, I. (2012). Chapter nine - Methods for cell and particle tracking. *Methods Enzymol.* **504**, 183-200. doi:10.1016/B978-0-12-391857-4.00009-4

Nagano, A., Koga, R., Ogawa, M., Kurano, Y., Kawada, J., Okada, R., Hayashi, Y. K., Tsukahara, T. and Arahata, K. (1996). Emerin deficiency at the nuclear membrane in patients with Emery-Dreifuss muscular dystrophy. *Nat. Genet.* **12**, 254-259. doi:10.1038/ng0396-254

Nava, M. M., Miroshnikova, Y. A., Biggs, L. C., Whitefield, D. B., Metge, F., Boucas, J., Vihinen, H., Jokitalo, E., Li, X., García Arcos, J. M. et al. (2020). Heterochromatin-driven nuclear softening protects the genome against mechanical stress-induced damage. *Cell* **181**, 800-817.e22. doi:10.1016/j.cell.2020.03.052

Ouyang, M., Sun, J., Chien, S. and Wang, Y. (2008). Determination of hierarchical relationship of Src and Rac at subcellular locations with FRET biosensors. *Proc. Natl. Acad. Sci. USA.* **105**, 14353-14358. doi:10.1073/pnas.0807537105

Paul, C. D., Mistriotis, P. and Konstantopoulos, K. (2017). Cancer cell motility: lessons from migration in confined spaces. *Nat. Rev. Cancer* **17**, 131-140. doi:10.1038/nrc.2016.123

Pfaff, J., Monroy, J. R., Jamieson, C., Rajanala, K., Vilardi, F., Schwappach, B. and Kehlenbach, R. H. (2016). Emery–Dreifuss muscular dystrophy mutations impair TRC40-mediated targeting of emerin to the inner nuclear membrane. *J. Cell Sci.* **129**, 502-516. doi:10.1242/jcs.179333

Raab, M., Gentili, M., de Belly, H., Thiam, H.-R., Vargas, P., Jimenez, A. J., Lautenschlaeger, F., Voituriez, R., Lennon-Duménil, A.-M., Manel, N. et al. (2016). ESCRT III repairs nuclear envelope ruptures during cell migration to limit DNA damage and cell death. *Science* **352**, 359-362. doi:10.1126/science.aad7611

Ruprecht, V., Wieser, S., Callan-Jones, A., Smutny, M., Morita, H., Sako, K., Barone, V., Ritsch-Marte, M., Sixt, M., Voituriez, R. et al. (2015). Cortical contractility triggers a stochastic switch to fast amoeboid cell motility. *Cell* **160**, 673-685. doi:10.1016/j.cell.2015.01.008

Stroka, K. M., Jiang, H., Chen, S.-H., Tong, Z., Wirtz, D., Sun, S. X. and Konstantopoulos, K. (2014). Water permeation drives tumor cell migration in confined microenvironments. *Cell* **157**, 611-623. doi:10.1016/j.cell.2014.02.052

Tozluoğlu, M., Tournier, A. L., Jenkins, R. P., Hooper, S., Bates, P. A. and Sahai, E. (2013). Matrix geometry determines optimal cancer cell migration strategy and modulates response to interventions. *Nat. Cell Biol.* **15**, 751-762. doi:10.1038/ncb2775

Ullo, M. F. and Logue, J. S. (2018). Re-thinking preclinical models of cancer metastasis. *Oncoscience* **5**, 252-253. doi:10.18632/oncoscience.450

Ungricht, R. and Kutay, U. (2017). Mechanisms and functions of nuclear envelope remodelling. *Nat. Rev. Mol. Cell Biol.* **18**, 229. doi:10.1038/nrm.2016.153

Venturini, V., Pezzano, F., Català Castro, F., Häkkinen, H.-M., Jiménez-Delgado, S., Colomer-Rosell, M., Marro, M., Tolosa-Ramon, Q., Paz-López, S., Valverde, M. A. et al. (2020). The nucleus measures shape changes for cellular proprioception to control dynamic cell behavior. *Science* **370**, eaba2644. doi:10.1126/science.aba2644

Verveer, P. J., Rocks, O., Harpur, A. G. and Bastiaens, P. I. H. (2006). Measuring FRET by acceptor photobleaching. *CSH Protoc.* **2006**, pdb.ip15. doi:10.1101/pdb.ip15

Webb, D. J., Donais, K., Whitmore, L. A., Thomas, S. M., Turner, C. E., Parsons, J. T. and Horwitz, A. F. (2004). FAK-Src signalling through paxillin, ERK and MLCK regulates adhesion disassembly. *Nat. Cell Biol.* **6**, 154-161. doi:10.1038/ncb1094

Yamada, K. M. and Sixt, M. (2019). Mechanisms of 3D cell migration. *Nat. Rev. Mol. Cell Biol.* **20**, 738-752. doi:10.1038/s41580-019-0172-9

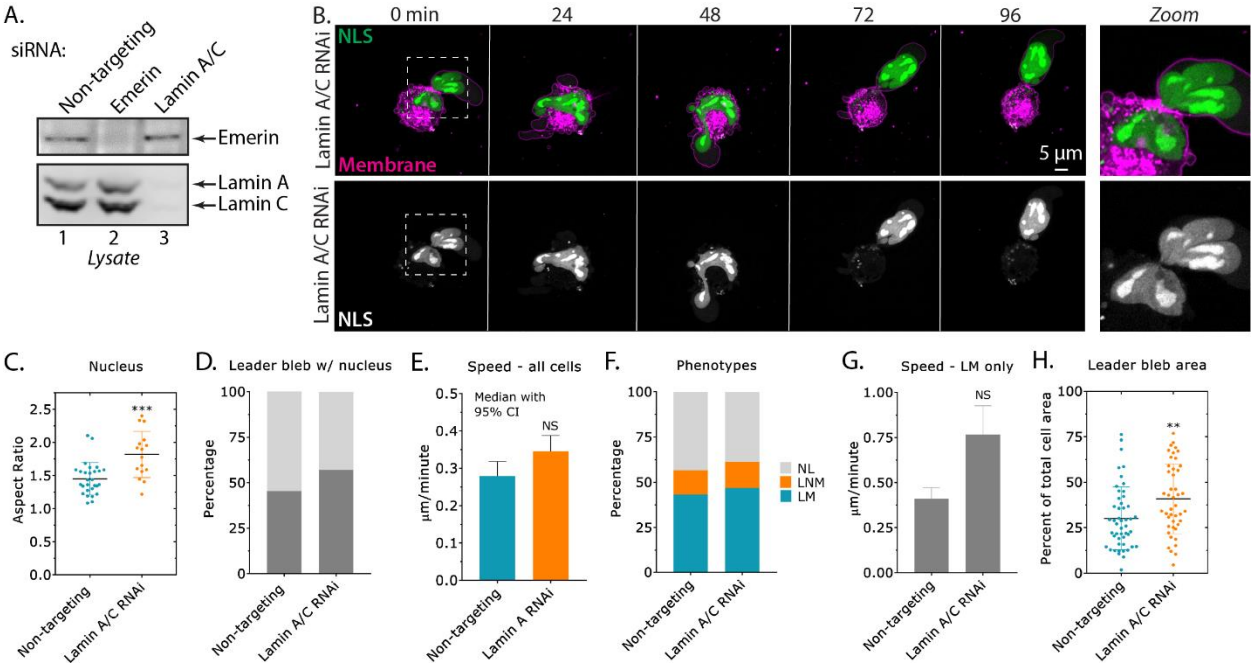

Fig. S1. **A.** Western blot confirmation of emerin and Lamin A/C RNAi in A375-M2 cells. Cells were treated for 5 days with each Locked Nucleic Acid (LNA; 50 nM) to achieve a near complete removal of each protein. **B.** Time-lapse imaging of a A375-M2 cell after Lamin A/C RNAi transiently transfected with Nuclear Localization Sequence (NLS) tagged mEmerald (NLS-mEmerald), which has been confined down to ~3 µm. Cells were stained with membrane dye. Zoom highlights nuclear shape changes in Lamin A/C RNAi cells. **C.** Nuclear aspect ratio for cells after Lamin A/C RNAi (mean +/- SD; two-tailed Student's t-test). **D.** Percent cells with leader blebs containing the nucleus in Lamin A/C RNAi cells. **E.** Instantaneous speeds for all cells after Lamin A/C RNAi (median +/- 95% CI; two-tailed Student's t-test). **F.** Percent NL, LNM, and LM for Lamin A/C RNAi cells. Statistical significance was determined using a Chi-squared test (χ^2=0.748). **G.** Instantaneous speeds for leader mobile (LM) cells after Lamin A/C RNAi (mean +/- SEM; two-tailed Student's t-test). **H.** Leader bleb area (calculated as the percent of total cell area) for cells after Lamin A/C RNAi
(mean +/- SD; two-tailed Student's t-test). All data are representative of at least three independent experiments. * - $p \leq 0.05$, ** - $p \leq 0.01$, *** - $p \leq 0.001$, and **** - $p \leq 0.0001$

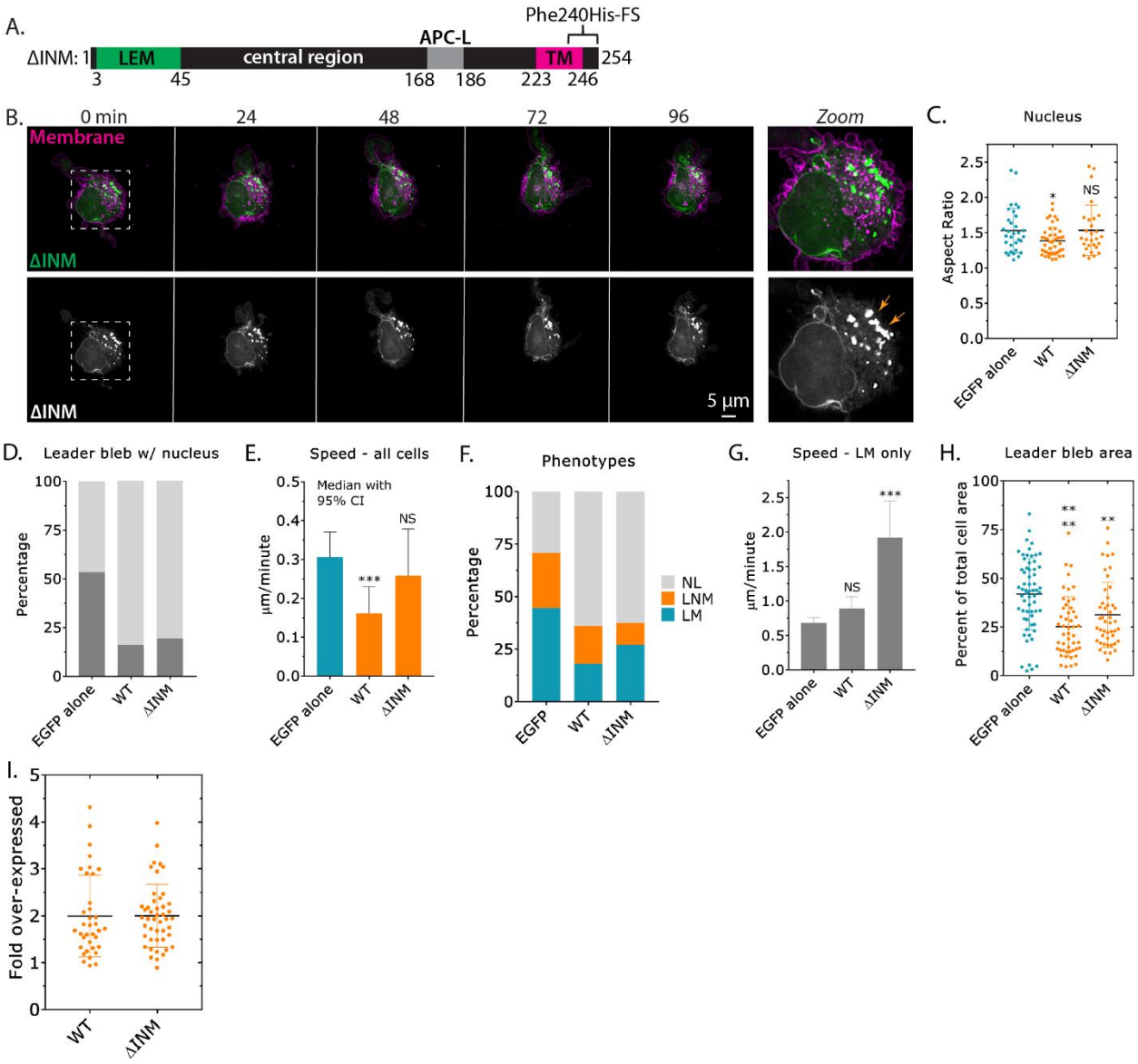

Fig. S2. **A.** Cartoon of the previously described frame shift mutation, Phe240His-FS, near the transmembrane (TM) domain for retaining emerin within the ONM/ER (ΔINM). LEM (Lap2, emerin, MAN1) domain and APC-like (APC-L) domain. **B.** Time-lapse imaging of a A375-M2 cell transiently transfected with emerin-EGFP (ΔINM), which has been confined down to ~3 µm. Cells were stained with membrane dye. Zoom shows emerin (ΔINM) predominantly at the ONM/ER. **C.** Nuclear aspect ratio of cells over-expressing (OE) EGFP alone, emerin WT, and ΔINM (mean +/- SD; multiple-comparison test post-hoc). **D.** Percent cells with leader blebs containing the nucleus for EGFP alone, emerin WT, and ΔINM. **E.** Instantaneous speeds for all cells over-expressing (OE) EGFP alone, emerin WT, and ΔINM. **F.** Percent NL, LNM, and LM for EGFP alone, emerin WT, and ΔINM. Statistical significance was determined using a Chi-squared test (EGFP alone vs. ΔINM; χ^2=2.42 x 10^{-15}). **G.** Instantaneous speeds for leader mobile (LM) cells over-expressing (OE) EGFP alone, emerin WT, and ΔINM (mean +/- SEM;

multiple-comparison test post-hoc). **H.** Leader bleb area (calculated as the percent of total cell area) for cells over-expressing (OE) EGFP alone, emerin WT, and ΔINM (mean +/- SD; multiple-comparison test post-hoc). **I.** Immunofluorescence (IF) was used to conduct a cell-by-cell analysis of emerin WT and ΔINM over-expression (OE; mean +/- SD). All data are representative of at least three independent experiments. * - $p \leq 0.05$, ** - $p \leq 0.01$, *** - $p \leq 0.001$, and **** - $p \leq 0.0001$

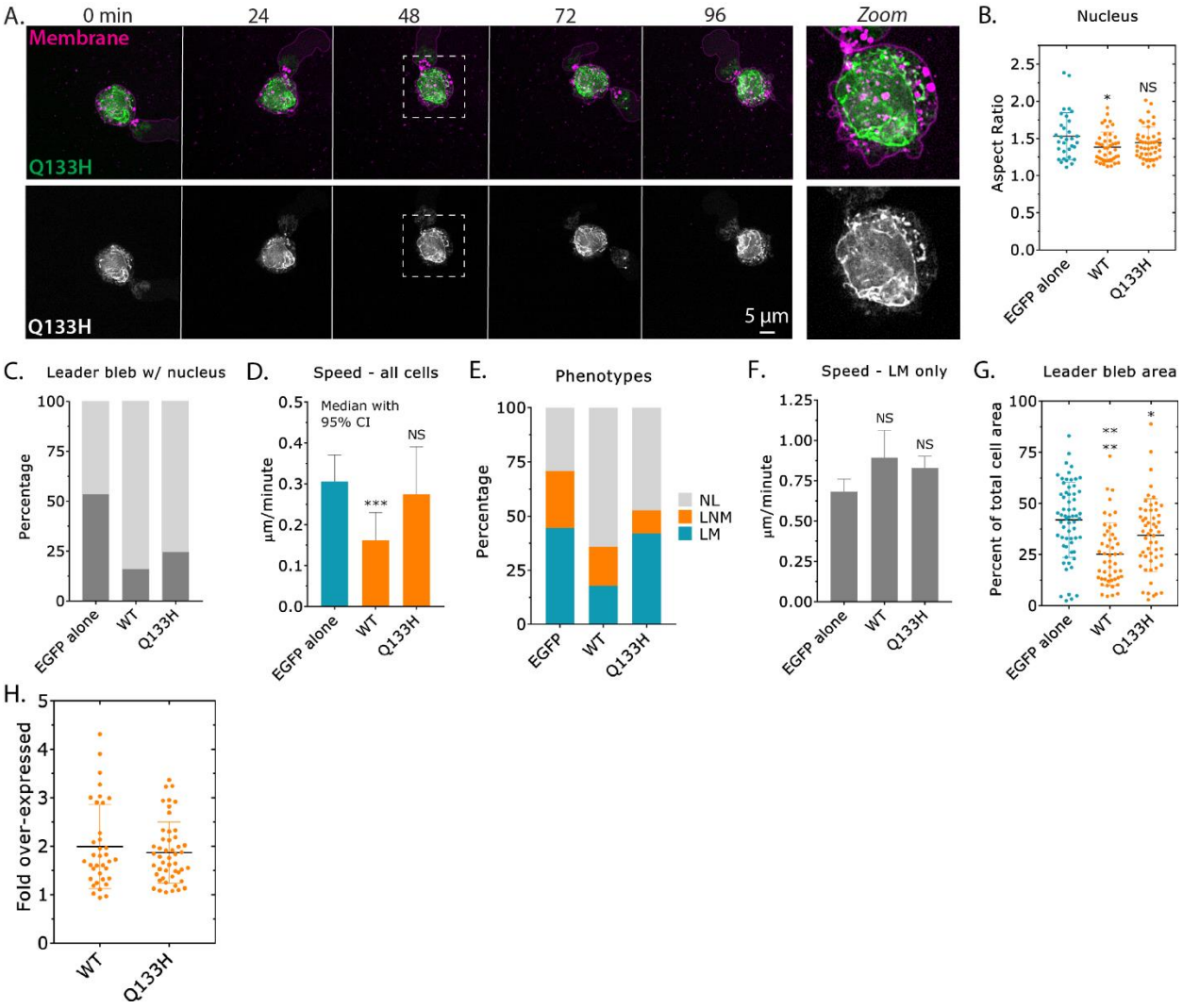

Fig. S3. **A.** Time-lapse imaging of a A375-M2 cell transiently transfected with emerin-EGFP (Q133H), which has been confined down to ~3 µm. Cells were stained with membrane dye. Zoom shows emerin (Q133H) predominantly at the nuclear envelope and ER. **B.** Nuclear aspect ratio for cells over-expressing (OE) EGFP alone, emerin WT, and Q133H (mean +/- SD; multiple-comparison test post-hoc). **C.** Percent cells with leader blebs containing the nucleus for EGFP alone, emerin WT, and Q133H. **D.** Instantaneous speeds for all cells over-expressing (OE) EGFP alone, emerin WT, and Q133H (median +/- 95% CI; multiple-comparison test post-hoc). **E.** Percent NL, LNM, and LM for EGFP alone, emerin WT, and Q133H. Statistical significance was determined using a Chi-squared test (EGFP alone vs. Q133H; $\chi^2=5.07 \times 10^{-6}$). **F.** Instantaneous speeds for leader mobile (LM) cells over-expressing (OE) EGFP alone, emerin WT, and Q133H (mean +/- SEM; multiple-comparison test post-hoc). **G.** Leader bleb area (calculated as the percent of total cell area) for cells over-expressing (OE) EGFP alone, emerin WT, and Q133H (mean +/- SD; multiple-comparison test post-hoc). **H.** IF was used to conduct a cell-by-cell analysis of emerin WT and Q133H over-expression (OE; mean +/- SD). All data are representative of at least three independent experiments. * - $p \leq 0.05$, ** - $p \leq 0.01$, *** - $p \leq 0.001$, and **** - $p \leq 0.0001$

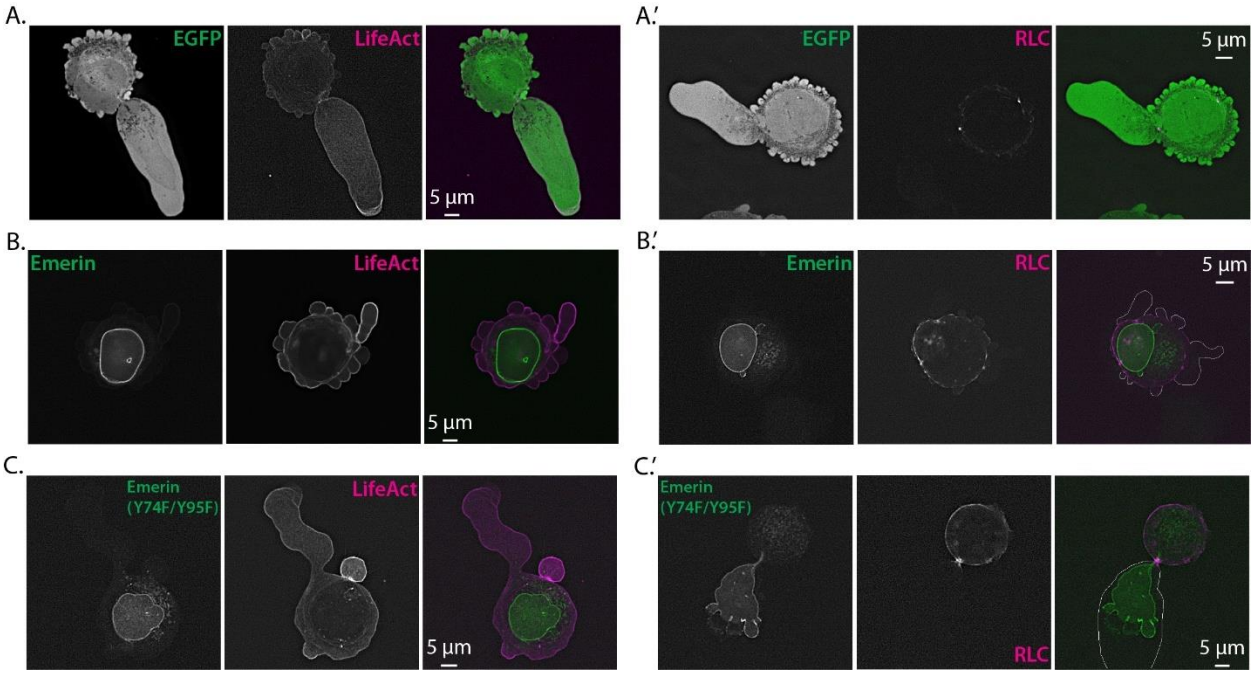

Fig. S4. A. - A.' Representative images of an A375-M2 cell confined down to ~3 µm with (A) EGFP alone and mScarlet-LifeAct and (A') EGFP alone and tdTomato-Regulatory Light Chain (RLC). **B. - B.'** Representative images of an A375-M2 cell confined down to ~3 µm with (B) emerin-EGFP and mScarlet-LifeAct and (B') emerin-EGFP and tdTomato-RLC. The cell boundary was outlined in B'. **C. - C.'** Representative images of an A375-M2 cell confined down to ~3 µm with (C) emerin-EGFP (Y74F/Y95F) and mScarlet-LifeAct and (C') emerin-EGFP (Y74F/Y95F) and tdTomato-RLC. The cell boundary was outlined in C'. All data are representative of at least three independent experiments.

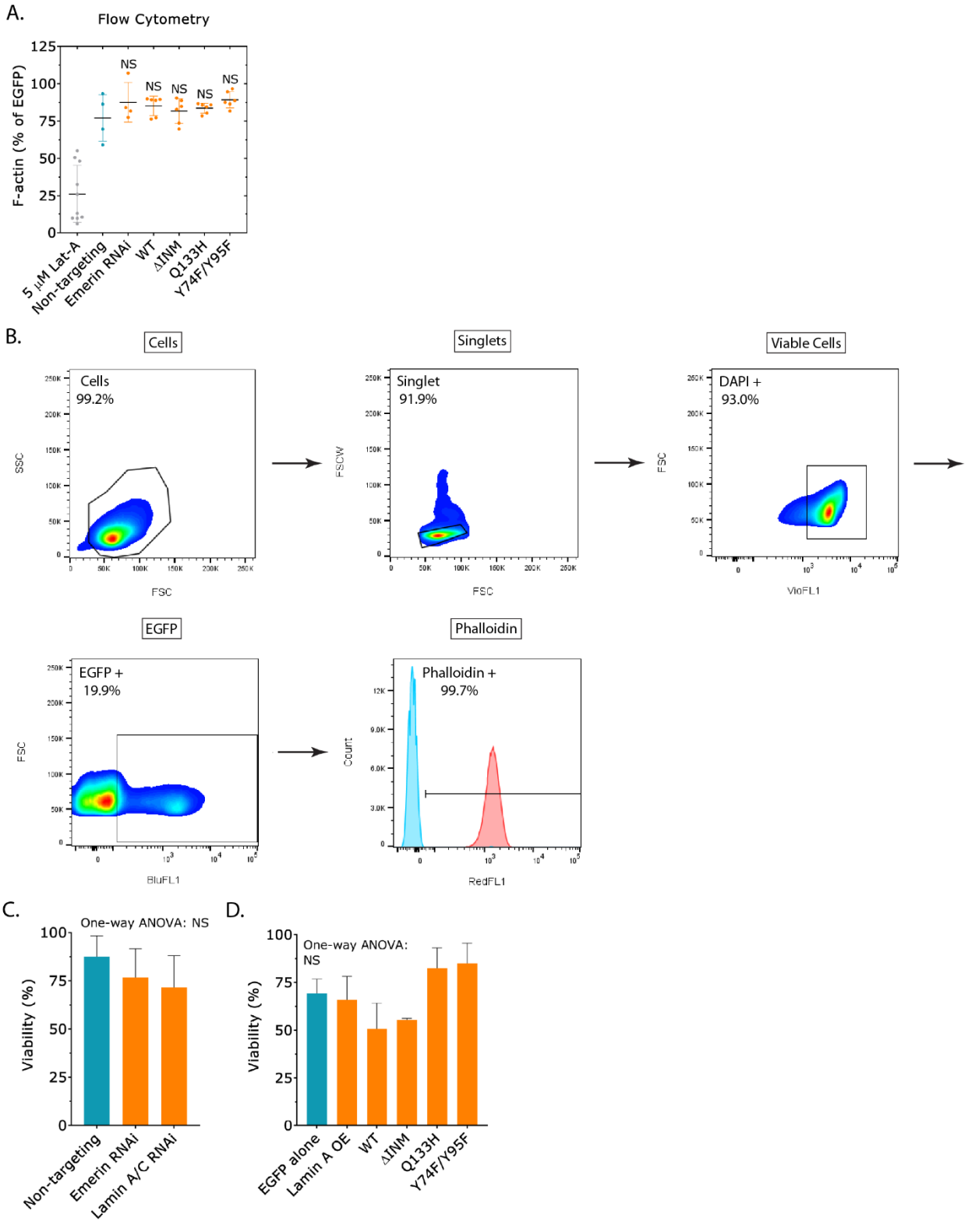

Fig. S5. A. Flow cytometry analysis of total F-actin, as measured by far red fluorescent phalloidin binding in cells treated with Latrunculin-A (Lat-A; 5 µM), non-targeting, emerin RNAi, over-expressing (OE) emerin WT, ΔINM, Q133H, and Y74F/Y95F (relative to EGFP alone) (mean +/- SD; multiple-comparison test post-hoc). Each point corresponds to a Median Fluorescence Intensity (MFI). **B.** Flow gating strategy. Cells are isolated based on instrument calibration. Single cells were isolated by comparing forward scatter width and height. Viable cells were identified using DAPI staining while EGFP fluorescence was used to identify transfected cells. Cells that were positively stained with phalloidin (red curve) were isolated based on a gate created referencing unstained cells (blue curve) for analysis. **C.** Percent A375-M2 cells confined down to ~3 µm alive after 5 hr of fluorescence imaging after non-targeting, emerin, and Lamin A/C RNAi (mean +/- SEM; One-way ANOVA). **D.** Percent A375-M2 cells confined down to ~3 µm alive (viability) after 5 hr of fluorescence imaging over-expressing (OE) EGFP alone, Lamin A, emerin WT, ΔINM, Q133H, and Y74F/Y95F (mean +/- SEM; One-way ANOVA). All data are representative of at least three independent experiments. * - $p \leq 0.05$, ** - $p \leq 0.01$, *** - $p \leq 0.001$, and **** - $p \leq 0.0001$

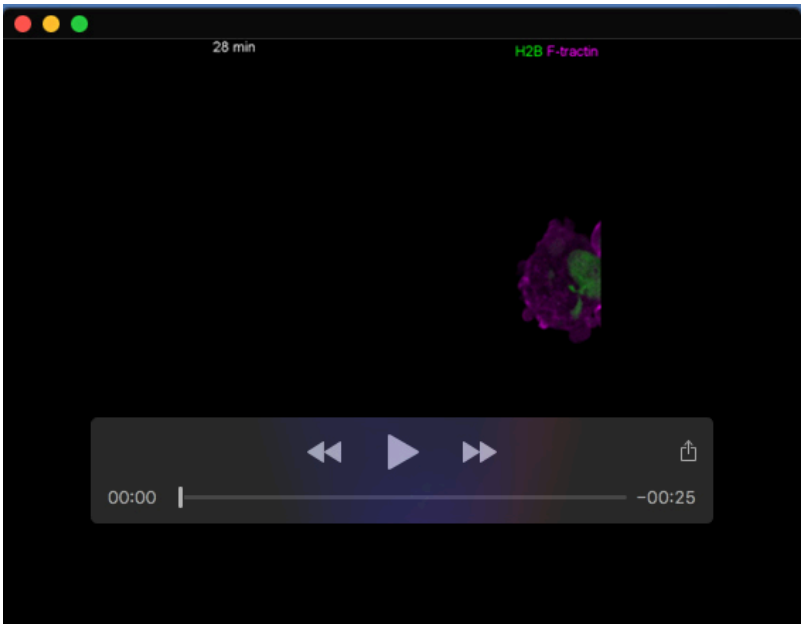

Movie 1. Time-lapse imaging of a leader mobile (LM) cell transiently transfected with H2B-mEmerald and F-tractin-FusionRed, which has been confined down to ~3 µm.

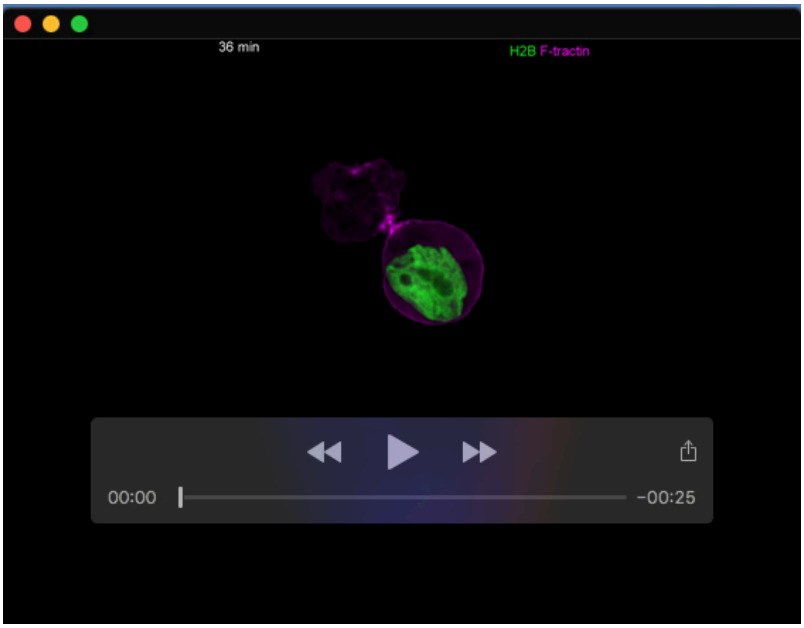

Movie 2. Time-lapse imaging of a leader non-mobile (LNM) cell transiently transfected with H2B-mEmerald and F-tractin-FusionRed, which has been confined down to ~3 µm.

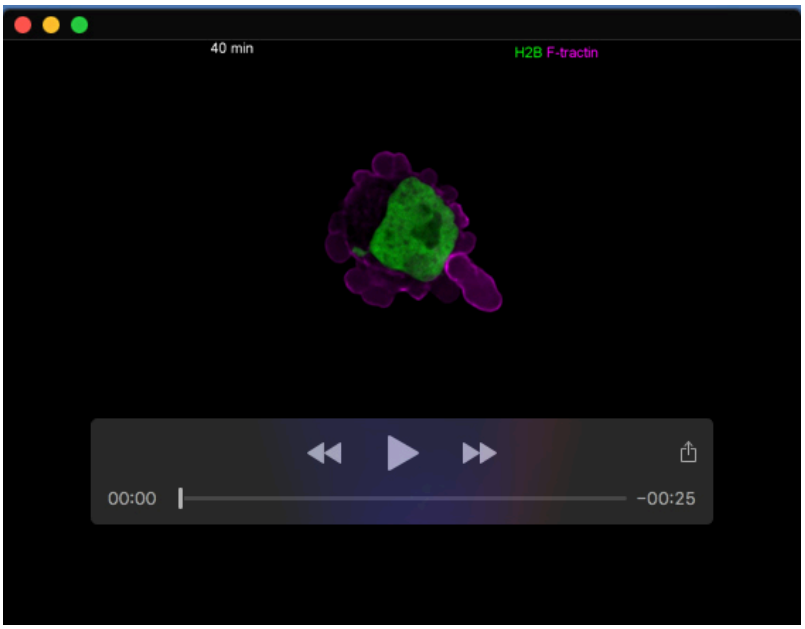

Movie 3. Time-lapse imaging of a no leader (NL) cell transiently transfected with H2B-mEmerald and F-tractin-FusionRed, which has been confined down to ~3 µm.

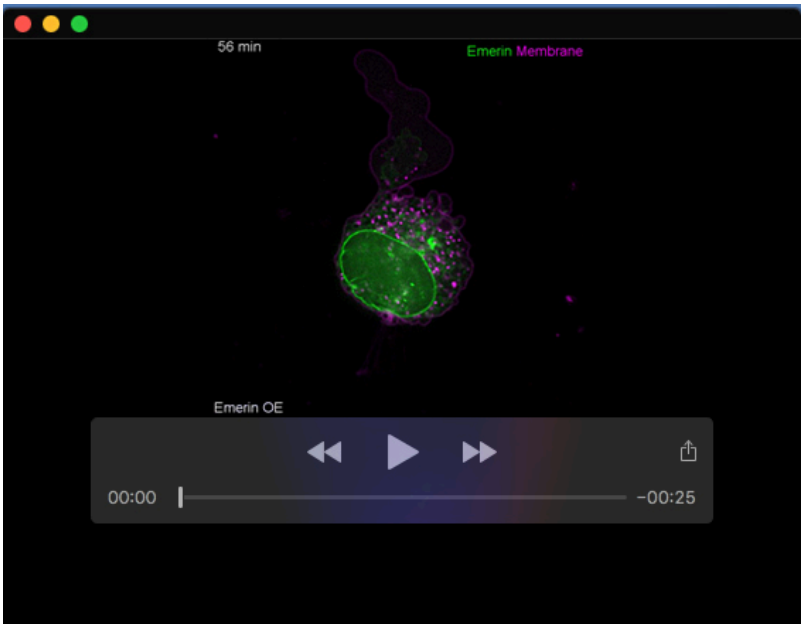

Movie 4. Time-lapse imaging of an A375-M2 cell over-expressing (OE) emerin-EGFP, which has been confined down to ~3 µm. Cells were stained with membrane dye.

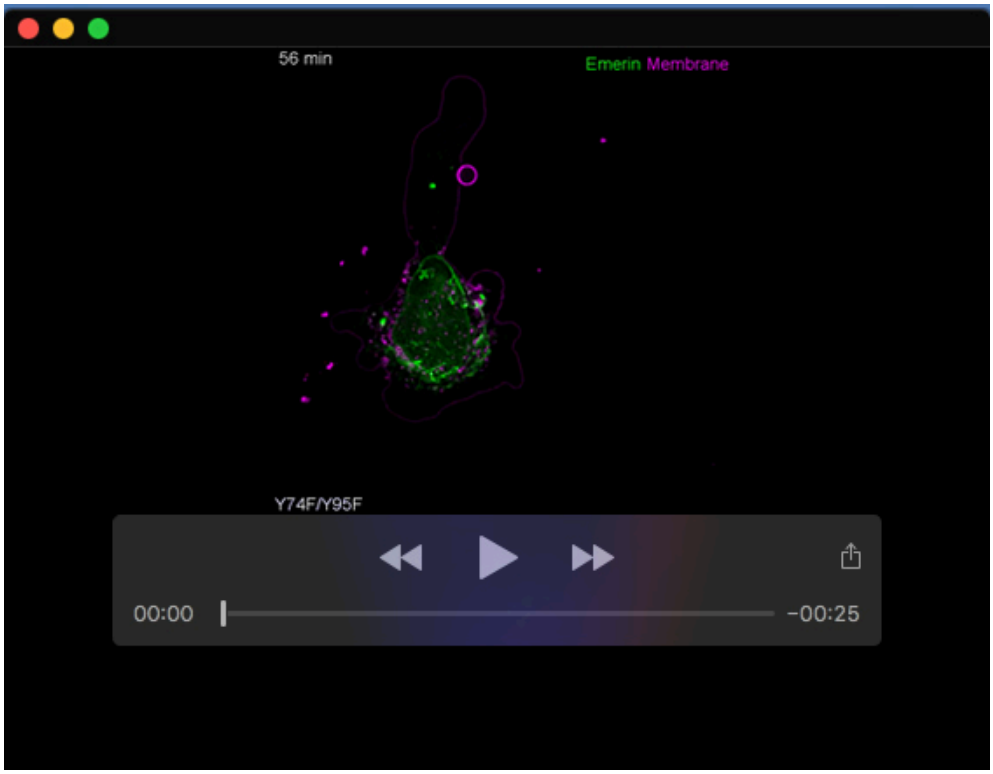

Movie 5. Time-lapse imaging of an A375-M2 cell over-expressing (OE) emerin-EGFP (Y74F/Y95F), which has been confined down to ~3 µm. Cells were stained with membrane dye.